Cell Rep. Author manuscript; available in PMC: 2023 Sep 15.
Published in final edited form as: Cell Rep. 2022 Sep 6;40(10):111279. doi: 10.1016/j.celrep.2022.111279

Artificial Gravity Partially Protects Space-induced Neurological Deficits in *Drosophila melanogaster*

Siddhita D Mhatre [1,2,3,12], Janani Iyer [1,2,4,12], Juli Petereit [5], Roberta M Dolling-Boreham [6,7], Anastasia Tyryshkina [8], Amber Paul [1,9], Rachel Gilbert [1,9], Matthew Jensen [8], Rebekah J Woolsey [10], Sulekha Anand [11], Marianne B Sowa [1], David R Quilici [10], Sylvain V Costes [1], Santhosh Girirajan [8], Sharmila Bhattacharya [1,13,*]

Author information
PMCID: PMC10503492 NIHMSID: NIHMS1881633 PMID: 36070701

Summary

Spaceflight poses risks to the central nervous system (CNS), and understanding neurological responses is important for future missions. We report CNS changes in *Drosophila* aboard the International Space Station in response to microgravity (SFμg) and artificially simulated Earth gravity (SF1g) *via* inflight centrifugation as a countermeasure. While inflight behavioral analyses of SFμg exhibit increased activity, postflight analysis displays significant climbing defects, highlighting the sensitivity of behavior to altered gravity. Multi-omics analysis shows alterations in metabolic, oxidative stress, and synaptic transmission pathways in both SFμg and SF1g; however, neurological changes immediately postflight, including neuronal loss, glial cell count alterations, oxidative damage, and apoptosis, are seen

only in SFμg. Additionally, progressive neuronal loss and a glial phenotype in SF1g and SFμg brains, with pronounced phenotypes in SFμg, are seen upon acclimation to Earth conditions. Overall, our results indicate that artificial gravity partially protects the CNS from the adverse effects of spaceflight.

Introduction

Exploration missions to the Moon and Mars would expose astronauts to environmental challenges, including gravitational changes, ionizing radiation, altered circadian rhythm, elevated CO_2, and isolation. Human acclimation to these environments presents complex health effects, with acute and prolonged consequences in multiple tissues that may result in increased risk to crew health and performance during the mission (Afshinnekoo et al., 2020; Crucian et al., 2015; Garrett-Bakelman et al., 2019; Grimm et al., 2016; Indo et al., 2016; Kononikhin et al., 2017; Wilson et al., 2018). With a high concentration of oxidizable, unsaturated lipids, low levels of antioxidant defenses, and high energy demand, the central nervous system (CNS) is particularly vulnerable to space stressors, with studies reporting behavioral deficits in spatial orientation, coordination, and locomotion, as well as cognition (Cekanaviciute et al., 2018; Clément et al., 2020, Salim, 2017, Friedman, 2011).

Spanning over 60 years of research, the short-term impacts of spaceflight on the CNS have been investigated, but there is still insufficient data regarding its long-term health risks (Clément et al., 2020). Also, there are limitations to evaluating the impact of CNS damage in humans. Therefore, there is a need to leverage research approaches using animal models that would aid in cellular, molecular, and mechanistic understanding of CNS responses to spaceflight. Recent literature has established the fruit fly as a valuable model for understanding the effects of microgravity (μg), hypergravity, and radiation in the spaceflight environment (Hateley et al., 2016; Hosamani et al., 2016; Ikenaga et al., 1997; Marcu et al., 2011; Ogneva et al., 2016). With their small size, short generation time (~10 days), short lifespan (~60-80 days), large number of offspring, and low cost of rearing, flies mitigate many of the practical concerns stemming from performing long term, multigenerational studies in space.

Here, we present the results of an International Space Station (ISS)-based study, MVPFly-01(Multi-use Variable-gravity Platform), to understand the effects of spaceflight on the fly nervous system and the value of artificial gravity (AG) as a countermeasure. AG is an attractive countermeasure, since it can potentially ameliorate the effect of microgravity (μg) on multiple physiological systems, by simulating Earth-like gravity (Clément, 2017; Clément and Traon, 2004; Horie et al., 2019; Shiba et al., 2017; Young, 1999). We performed behavioral analyses, brain immunohistochemistry, proteomics, and transcriptomics on flies subjected to microgravity (SFμg), inflight artificially simulated Earth gravity (SF1g), and environmentally matched ground control (Earth). Our results showed inflight and postflight behavioral changes and morphological alterations in the brain immediately postflight in response to μg. Further, acclimation to Earth following spaceflight revealed brain morphological changes in both SF1g and SFμg flies, with pronounced phenotypes in SFμg. These results, in combination with metabolic pathways altered in transcriptomic and proteomic studies on fly heads frozen on the ISS provide comprehensive information on the effects of inflight AG exposure on

CNS and postflight acclimation to Earth conditions.

Results

The MVP-Fly-01 mission

The ISS is a useful environment for studying the effects of spaceflight by combining a μg environment with ionizing radiation and CO_2 levels that are elevated compared to Earth's surface (McDonald et al., 2020). The MVP-Fly-01 validation mission (34 days) has enabled comprehensive investigations of the fly CNS (Figure 1A). The two inflight centrifuges in the MVP hardware allowed us to maintain one centrifuge at μg (SFμg) with the flies developing entirely in μg, while the other centrifuge simulated Earth's gravitational force (SF1g) on ISS and acted as a high-fidelity on-orbit control for gravity. In other words, the spaceflown flies experienced identical environmental perturbations during take-off and landing, were maintained in identical hardware, similar gas composition, sound pressure levels, temperature, and radiation environments in space, but were reared either under a 1g force in space or in μg. Upon completing the mission, a postflight ground control experiment was performed on Earth (Earth) using the same flight hardware and precisely simulating spaceflight conditions. The flies retrieved upon completion of the mission were used for behavioral, morphological, and acclimation analyses to study the effects of spaceflight on the CNS (Figure 1B).

Figure 1: Inflight behavioral analysis shows hyperactivity in microgravity.

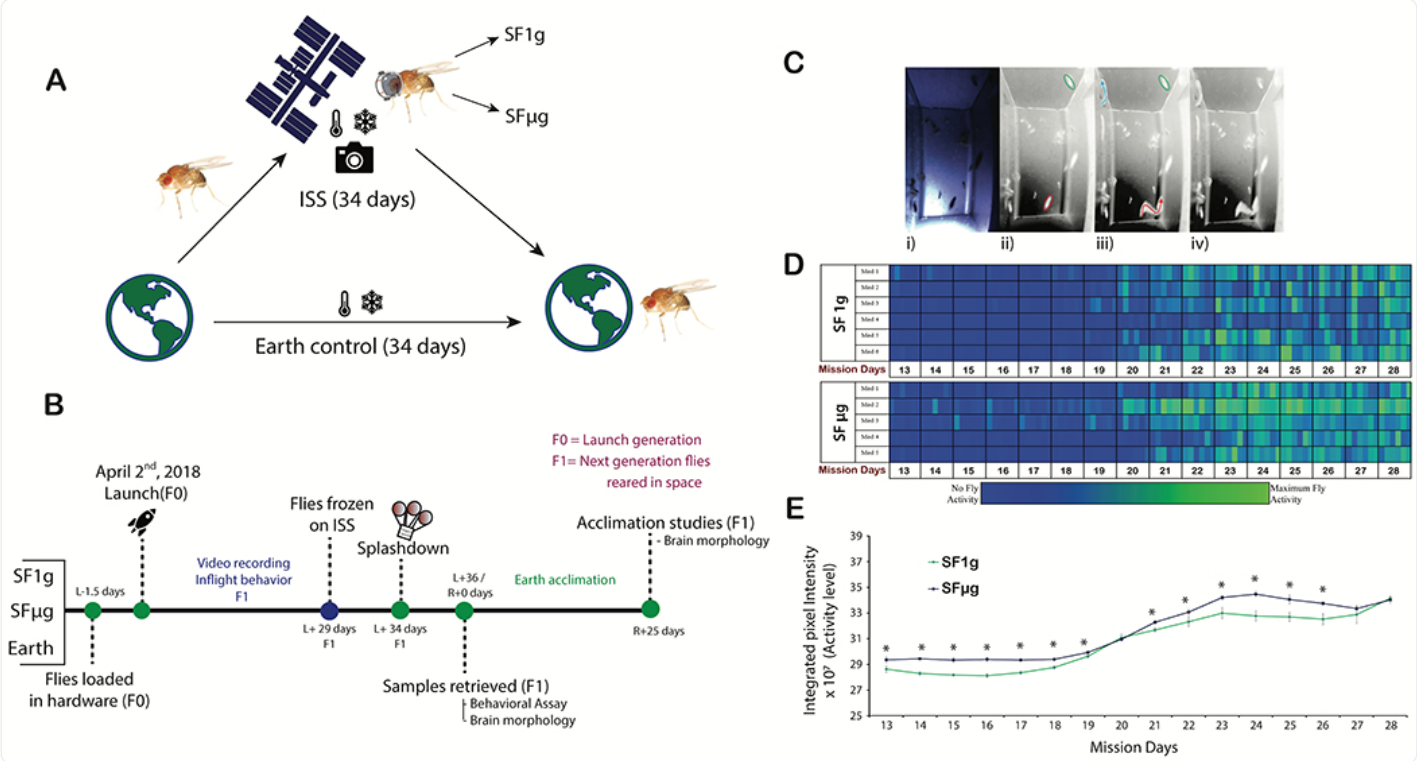

Open in a new tab

(A) Schematic of MVP-Fly01 mission outline depicting the 34-days mission on ISS. Camera represents inflight videos that were recorded to monitor fly health and behavior. Onboard operations included freezing the food cylinders containing flies and larvae in RNAlater for omics analysis. Live flies were returned to Earth. Following the telemetry and timeline of the mission, matched Earth controls were performed (Earth). (B) Experimental timeline highlighting the onboard operations and postflight R+0 and R+25 assays. (C) Computation of fly activity by MIP. i) The first frame from one video recorded during the mission. ii) The negative of the blue channel in grayscale of the first frame with two flies circled in green and red. iii) The MIP image captures the movement (blue and red arrows) and no movement (green) of the flies. iv) Final MIP projection used in the algorithm. The white tracks represent flies that moved at any point during the recording. (D) Fly activity mapped overtime for 16 days (mission day 13-28). Each row represents one adult fly chamber in an individual MVP module, and across from left to right is a temporal progression with every six rectangles (each rectangle = 28s video recording) spanning a single 12-hr light period. The color bar represents the activity level from a minimum background intensity (dark blue) to the highest activity level intensity (bright green). Top six rows correspond to SF1g flies and bottom five to SFµg flies. (E) Line graphs show increased activity levels across mission day 13-28 averaged over each day across modules for each population set (n=5-73). *$p<0.05$.

SFµg flies exhibit increased activity on ISS

We developed an automated quantification algorithm that computes the maximum intensity projections (MIPs) of video recordings of fly behavior (represented in Videos S1 and S2) during spaceflight and sums pixel intensities to produce numerical values representative of fly activity levels (higher numerical values correlate with high fly activity), accounting for both the emergence of flies and their movement during the 12-hr light period (Figure 1C). Since the fly population sizes in adult fly chamber 1 were not statistically different between SF1g and SFµg (Figure S2), any difference in MIP intensity between these two groups reflected differences in fly activity. We generated a color map showing the relative numerical activity in adult fly chamber 1 as a function of mission timeline (days 13-28) for each module grouped as either SF1g or SFµg (Figure 1D). Upon quantification, we found that the overall activity level of the SF1g flies is significantly below SFµg flies (Figure 1E). On mission day 20 and 28, there is no distinguishable difference in the activity for the two gravity levels. This is possibly due to the initial emergence of flies into the adult fly chamber around day 20 that causes a similar increase in activity in both SF1g and SFµg environments. On day 28, the high density of flies in both conditions may result in close proximity of the flies, thereby increasing their activity levels. The results show that within the closely matched fly populations maintained in spaceflight, flies exposed to µg conditions show significantly greater levels of activity than their 1g counterparts.

Flies exposed to microgravity conditions show behavioral and neuronal deficits, glial alterations, oxidative damage, and apoptosis

Upon landing, a subset of F1 flies were first used for behavioral assays to measure climbing ability. Climbing ability is the fly's innate negative geotactic response and is routinely used to assess nervous system dysfunction in fly models (Chakraborty et al., 2011; Iijima et al., 2004). This behavior relies on the integrity of the connection between the brain and muscles. Specifically, it involves the mushroom body, which is the part of the brain that regulates the transition from rest to responsiveness in relation to environmental stressors (Martin et al., 1998). To capture the sexually dimorphic responses, we assessed males and females separately in our analysis. We observed that males born in µg were more affected with significant deficits in climbing ability compared to Earth males (Figure 2A). A decreasing trend was also observed in SFµg females and SF1g (males and females) compared to their respective Earth control. Additionally, we noted a significant decrease in climbing ability in SFµg males compared to SFµg females. This result is consistent with the previously observed reduction in postflight climbing response in males exposed to µg (Benguría et al., 1996).

Figure 2: CNS-associated deficits in microgravity flies.

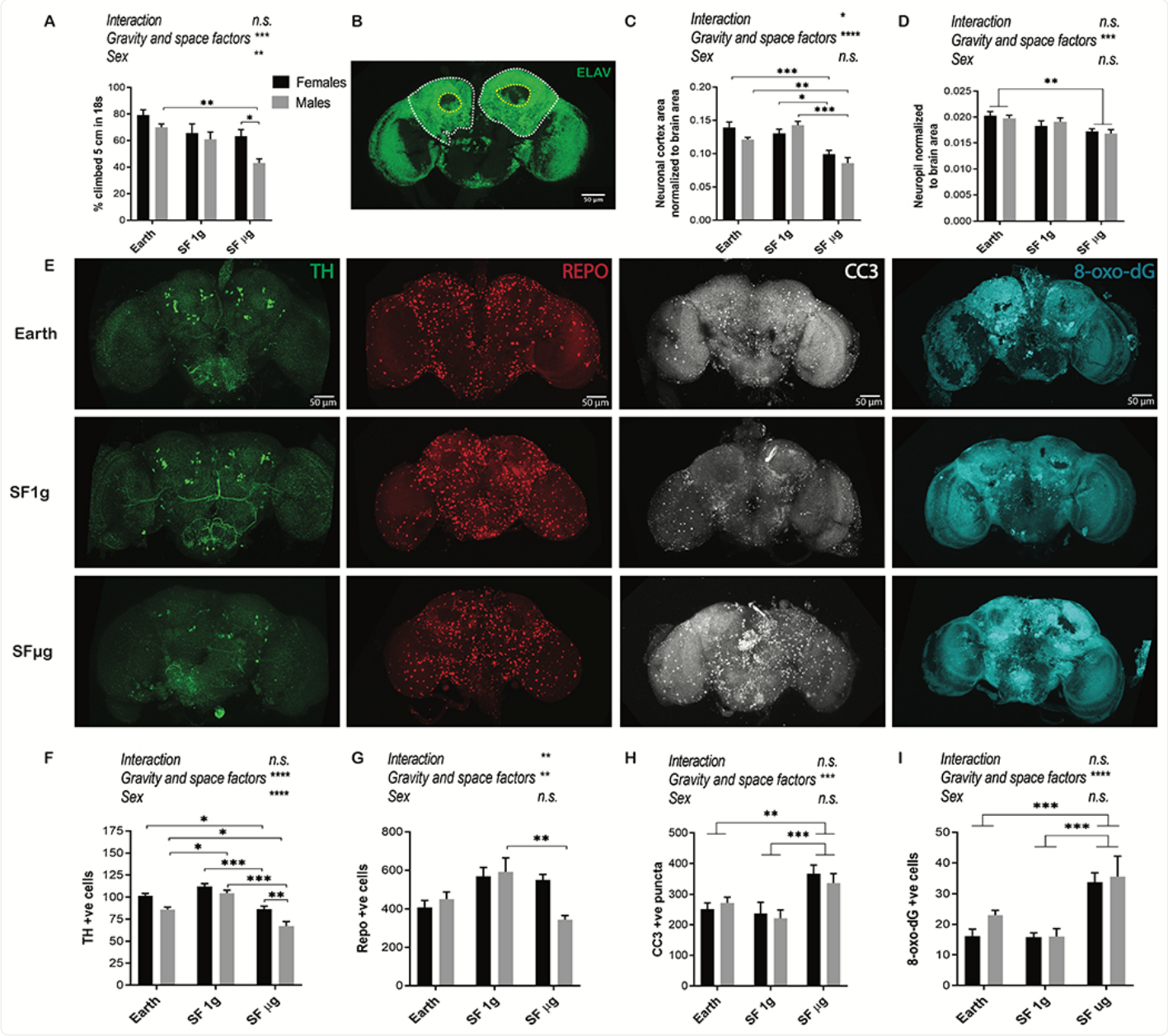

Open in a new tab

(A) Decreased climbing ability of space-flown flies (n=90-120). (B) Representative image of fly brain stained with neuronal marker, anti-ELAV; neuronal cortex marked by the dashed outer white line and neuropil marked by the dashed inner yellow line. Quantification shows decrease in neuronal cortex area (C) and neuropil area (D) in SFµg compared to both Earth and SF1g controls (n=10-14). (E) Representative images of fly brains labeled with anti-TH (green), anti-REPO (red), anti-CC3 (white), and anti-8-oxo-dG (cyan). Quantification showed significant loss in DA neurons (F) (n=6-9) and alterations in glial numbers (G) (n=5-9), apoptosis (H)

(n=5-7), and oxidative DNA damage (I) (n=5-7) in SFµg condition. Two-way ANOVA results are displayed above the histogram. Significance calculated by post-hoc test is represented as *p<0.05; **p<0.01; *** p<0.001.

We then dissected the adult fly brains and stained them with neuronal (anti-ELAV) (Figure 2B), apoptotic (anti-CC3), and oxidative stress-associated DNA damage (anti-8-oxo-dG) (Figure 2E) markers. Upon quantification, we observed a slight yet significant reduction in the total brain area of SFµg female flies compared to both Earth and SF1g females; males showed no change in brain sizes (Figure S3A). Morphological quantification with anti-ELAV staining showed a significant decrease in neuronal cortex area (Figure 2B, C, and S3B) in SFµg flies compared to Earth and SF1g control flies in both sexes. Similarly, the neuropil area is significantly reduced in SFµg compared to Earth flies (Figure 2D). A similar phenotype was noted in the Alzheimer's disease fly model accompanied with behavioral deficits (Mhatre et al., 2014). No significant differences in neuronal cortex and neuropil areas were observed in SF1g compared to Earth flies (Figure 2C, D). A marked increase in CC3 positive apoptotic puncta (Figure 2E, H) and 8-oxo-dG positive cells (Figure 2E, I) was observed in flies subjected to SFµg as compared to Earth and SF1g controls. Apoptotic cells were detected throughout the brain, and many of them colocalized with the ELAV marker (Figure S3Cv). Additionally, all the 8-oxo-dG positive cells colocalize with neuronal ELAV marker, suggesting oxidative damage in neuronal cells (Figure S3Civ, marked with green arrowhead). The observed oxidative stress response has been documented in previous spaceflight and ground-based altered gravity studies in mice and flies (Hateley et al., 2016; Hosamani et al., 2016; Mao et al., 2016, 2018b, 2020; da Silveira et al., 2020).

Another subset of brains was stained with glial (anti-Repo), and dopaminergic neuron (anti-TH) (Figure 2E) markers. Gross analysis of the total number of dopaminergic (DA) neurons revealed a reduction in DA neuron count in SFµg compared to SF1g and Earth fly brains in both sexes (Figure 2E, F). Like the climbing behavior, we observed significantly lowered DA neurons in SFµg males compared to SFµg females suggesting sensitivity of male flies to µg. DA neurons are involved in locomotion, and the lack of these neurons have been identified in the development of Parkinson's disease in humans (Ryczko and Dubuc, 2017). We also observed a significant increase in DA neurons in SF1g males compared to the Earth males; this may be part of a phenotype resulting from exposure to a 1g centrifugal force on flies that are also perturbed by a combination of spaceflight stressors - ionizing radiation and elevated CO_2 levels. In the case of glia, SFµg females and SF1g (both males and females) displayed an increasing trend in glial cell number compared to Earth controls. However, the SFµg males showed a decreasing trend in the glial population compared to Earth males (Figure 2E, G), and a significant reduction in the glial population compared to SF1g males. Further experiments are necessary to study the sex specificity of the spaceflight effects and the underlying mechanisms contributing to these differences in glial cell populations.

The SF1g and Earth flies were exposed to similar temperature, humidity, CO_2, and sound pressure levels, however, ionizing radiation was an additional spaceflight stressor experienced by the SF1g flies compared to the Earth flies. Thus,

the similarity in morphological phenotype between SF1g and Earth control flies in many of the readouts analyzed here, including behavior, neuronal cortex and neuropil areas, apoptosis, and oxidative damage (Figure 2), suggests that radiation alone may not be a significant contributing factor for the immediate postflight CNS effects of spaceflight. However, ionizing radiation may contribute to some of the long-term effects of spaceflight on the CNS and are discussed further in a later section. The entire experiment occurred over a short duration (34 days) and the radiation environment in LEO is known to be more benign than the environment in deep space, beyond the Van Allen belts (Nelson, 2016). Therefore, the gross physiological changes induced in LEO flights like on ISS, as observed in SFµg flies, at least for the CNS immediately post-return, may primarily be associated with changes in gravity. Thus, these results indicate that gravity can play a key role in the LEO environment, causing neuronal and neurobehavioral deficits during spaceflight.

Global omics analysis highlights spaceflight induced altered genes and proteins in the brain

Transcriptomics and proteomics analyses were performed on the heads of flies which developed entirely on ISS under SFµg or SF1g conditions and Earth controls (Figure 3A). RNAseq on heads from SFµg flies compared with Earth controls showed differential expression of 1014 genes in females and 507 genes in males, while proteomics analysis revealed differential expression of 577 proteins in females and 719 proteins in males. RNAseq in SF1g flies compared to Earth reared flies showed differential expression of 80 genes in females and 601 genes in males, and proteomics analysis revealed differential expression of 389 proteins in females and 425 proteins in males (Figure 3A). Overall, these results suggest alterations in transcripts and protein levels when flies are reared in space conditions compared to Earth condition. A full list of DEGs and DEPs is provided in Supplementary data (.xls 1 and 2). Further, to understand the overlap across the transcriptomics and proteomics as well as across the different experimental conditions, we generated an UpSet diagram displaying top 30 intersections (Figure 3B). The overlap between the DEGs (orange dots and bars) and DEPs (green dots and bars) for the experimental conditions is shown, and across DEGs and DEPs are marked in black. Also shown are the genes and proteins unique to each condition (grey dots and bars). The intersection within DEPs across experimental conditions yields more hits compared to DEGs. This is evidenced by 167 significantly altered proteins (adj. p-value < 0.05), compared to 25 significantly altered genes (adj. p-value<0.05) in SF1g and SFµg conditions compared to Earth controls (Figures 3B and S4A, B). The observed overlapping DEPs and DEGs are potential spaceflight signatures irrespective of gravity that can be further investigated. Additionally, though we observe minimal overlap across both transcriptomic and proteomic platform, the common processes possibly share a transcriptional mechanism of dysregulation, hence making these processes central towards the phenotype manifested in spaceflight flies. For example, as shown in the case of SFµg female compared to Earth female, the gene ontology (GO) analysis of overlapping DEPs and DEGs (65) revealed enrichment of key biological processes (BP), cellular components (CC), and molecular functions (MF) that closely regulate mitochondrial functions, metabolic processes, immune response, and synaptic signaling, among others (Figure S4C).

Figure 3: Global overview of multi-omics analysis on flies frozen in space.

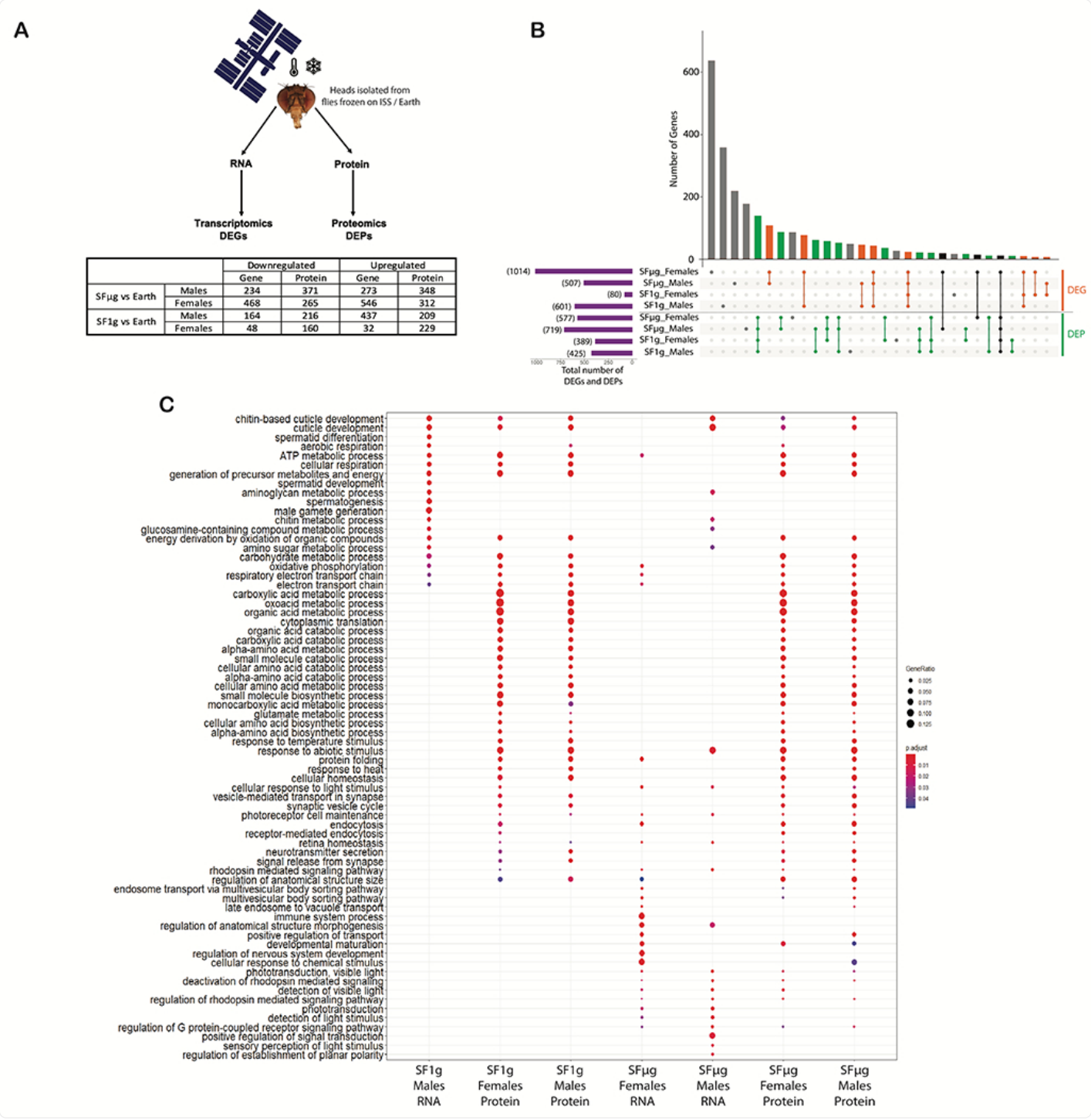

		Downregulated		Upregulated	
		Gene	Protein	Gene	Protein
SFµg vs Earth	Males	234	371	273	348
	Females	468	265	546	312
SF1g vs Earth	Males	164	216	437	209
	Females	48	160	32	229

Open in a new tab

(A) Schematic showing transcriptomics and proteomics sample processing. Table provides a global view of the total number of differentially up and down regulated genes (DEGs) and proteins (DEPs) in SF1g and SFµg compared to Earth control. (B) Upset plot displays top 30 intersections across omics platforms and

between conditions (SF1g males, SF1g females, SFµg males, SFµg females). The purple horizontal bars indicate the total number of DEGs and DEPs identified in each condition. The dotted region shows all conditions, connecting lines with black nodes show overlap across omics platforms (DEGs and DEPs), whereas orange nodes show overlap across different conditions in DEGs and green nodes show overlap across different conditions in DEPs. Grey nodes represent the DEGs and DEPs unique to a condition. The vertical bars indicate the number of unique or overlapping genes/proteins. (C) Dot plot representing top 20 significantly (adj.p-value <0.05) enriched gene ontology (GO) terms in biological processes in SF1g and SFµg compared to Earth control. SF1g female RNA compared to Earth control did not have any enriched GO biological processes, hence not represented in the dot plot. The color of the dot represents adj. p-value, and the size represents gene ratio.

Focused analysis reveals differential alteration in metabolic pathways and oxidative phosphorylation in space reared flies

The spaceflight conditions (SF1g and SFµg) compared to Earth were analyzed across the omics platforms. Figure 3C highlights the top 20 significantly enriched GO biological processes, including cuticle development, oxidative phosphorylation, electron transport chain, metabolic processes, response to heat, protein folding, neurotransmitter secretion, synaptic vesicle signaling, and retinal homeostasis, among others. The enrichment is more evident in proteins compared to RNA. The complete list from GO enrichment analysis (BP, CC, MF) is provided in Supplementary.xls 1 and 2. Further, we note a sexually dimorphic response in the transcriptomic dataset, which is not observed in proteomics analysis (Figure S5).

KEGG pathway enrichment analysis on the proteomics dataset across conditions revealed sexual dimorphism at the pathway enrichment level (more KEGG pathway enrichment in females than males), which was more evident in SF1g than SFµg condition. Proteomic data of SFµg flies (males and females) show enrichment of pathways such as endocytosis, cellular metabolic responsive pathways – tyrosine metabolism, sucrose metabolism, pyruvate metabolism, oxidative phosphorylation, carbon metabolism, glutamate metabolism, glycolysis, fatty acid metabolism, and amino acid metabolism (Figure 4A). These metabolic pathways play critical roles in cellular as well as mitochondrial homeostasis. The metabolic reprogramming under spaceflight conditions suggests metabolic and cellular stress, similar to that observed in cancer and aging (Brooks Robey et al., 2015; Wallace, 2005). Similar regulation of metabolic pathways is observed in other spaceflight-based mammalian studies, including humans (GarrettBakelman et al., 2019b; de Luca et al., 2009; da Silveira et al., 2020; Stein, 2002). Analysis of cellular respiration revealed perturbations in the biological processes and cellular components encompassing every step of the pathway, i.e., glucose metabolism, pyruvate metabolism, citric acid cycle (TCA), and electron transport chain as well as at mitochondrial organelle level (Figure 4B, C). This is observed in both spaceflight conditions but is more pronounced in SFµg than SF1g (both sexes), suggesting differential regulation under the spaceflight stress ± gravity vector.

Figure 4: Metabolic pathways and cellular respiration affected by spaceflight.

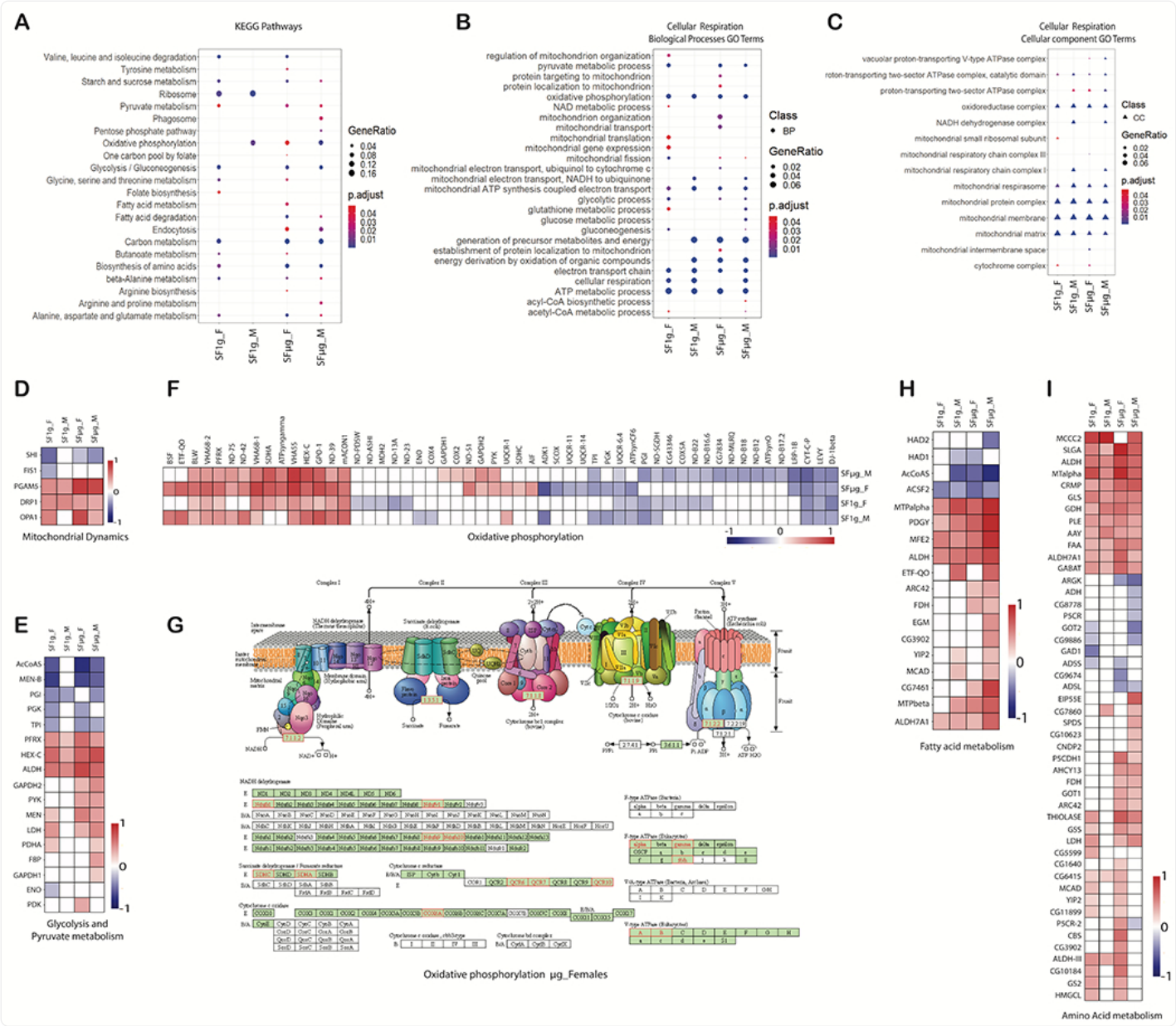

Open in a new tab

(A) Dot plot representing the KEGG pathways ($p<0.05$) enriched in DEPs across different conditions. The size of the dot is based on the gene count enriched in the pathways, and the color of the dot represents pathway significance. (B, C) GO enrichment analysis. Dot plot showing GO terms (adj. p-value<0.05) associated with cellular respiration in biological processes (B), and cellular components (C) for SF1g and SFμg (DEPs) compared to Earth control. The color of the dot represents adj. p-value, and the size represents gene ratio. (D-F) Heatmap representation of differential expression (log2[fold-change]) of significantly altered (adj. p-value<0.05) mitochondrial fusion/fission proteins (D), glycolysis and pyruvate metabolism

proteins (E), and proteins associated with oxidative phosphorylation (F) in SF1g and SFµg *vs.* Earth. (G) Differentially expressed proteins (in red) in SFµg females (*vs.* Earth females) are mapped onto the oxidative phosphorylation KEGG pathway using KEGG mapper. (H-I) Heatmap displays log2[fold-change] of proteins that are significantly expressed (adj. p-value<0.05) in fatty acid metabolism (H), and amino acid metabolism (I), with red representing upregulated and blue for downregulated.

At the mitochondrial level, an increase in PGAM5 and mitochondrial fission/fusion proteins such as dynamin-related protein 1 (DRP1) and OPA1 were observed, suggesting increased mitochondrial dynamics (Figure 4D). We observed the upregulation of many enzymes involved in glycolysis, such as hexokinase C (HEXC) and Fructose 1,6-bisphosphatase (FBP) (Figure 4E), suggesting increased glycolytic flux (Tanner et al., 2018). Meanwhile, we observed an increase in lactate dehydrogenase (LDH), suggesting funneling of glycolysis products towards lactate production under spaceflight conditions. Another key enzyme, AcCoAS, is downregulated, thereby reducing the production of Acetyl-CoA, a key enzyme required for the TCA cycle. Further, modulation of proteins involved in oxidative phosphorylation/ETC is noted (Figure 4F). While ETC proteins are differentially regulated under both SF1g and SFµg conditions, the number of proteins regulated under SFµg is more than the SF1g condition. In fact, differential regulation of at least one protein associated with each of the five ETC complexes is observed under SFµg conditions (Figure 4G), which may contribute to reactive oxygen species (ROS) production. Moreover, KEGG pathway enrichment shows differential regulation of fatty acid metabolism as well as amino acid metabolism. We observed an upregulation of enzymes involved in fatty acid (Figure 4H) and amino acid metabolism (Figure 4I), suggesting high energy demand, thereby emphasizing cellular stress response under spaceflight conditions (SFµg> SF1g).

Spaceflight alters the expression of stress-inducible proteins affecting CNS

During spaceflight, metabolic pathways are altered along with the biological processes associated with cellular stress, including response to heat, response to ROS, ROS metabolic process, and cellular homeostasis, thus indicating increased cellular stress (Figure 5A). We see significant upregulation of heat shock proteins (HSPs): HSP70AB, HSP26, HSP23, HSP27, and HSP67BC in both spaceflight conditions (Figure 5B). HSPs are the molecular chaperones with cytoprotective properties that are induced in response to a variety of cellular insults such as heat, radiation, oxidative stress, and altered gravity, to confer protection against deteriorating effects of ROS (Bukau et al., 2006; Hateley et al., 2016; Hosamani et al., 2016; Ikwegbue et al., 2018). Low amounts of ROS aid in neuronal development and function, but oxidative stress-induced excessive ROS levels lead to cellular damage, increased blood-brain barrier permeability, and altered brain morphology, causing neuroinflammation and neuronal death (Gu, 2011). Our observations of increased neuronal loss, apoptosis and oxidative damage in the fly brain further confirm the effects of oxidative stress during spaceflight (Figure 2). These morphological defects in the brain correlate with the altered expression of proteins that are enriched in functions such as neuronal projection, neuron death, axonogenesis, and synaptic transmission in SFµg flies compared to Earth (Figure 5C).

Figure 5: Increased cellular stress affects neuronal signaling in spaceflight.

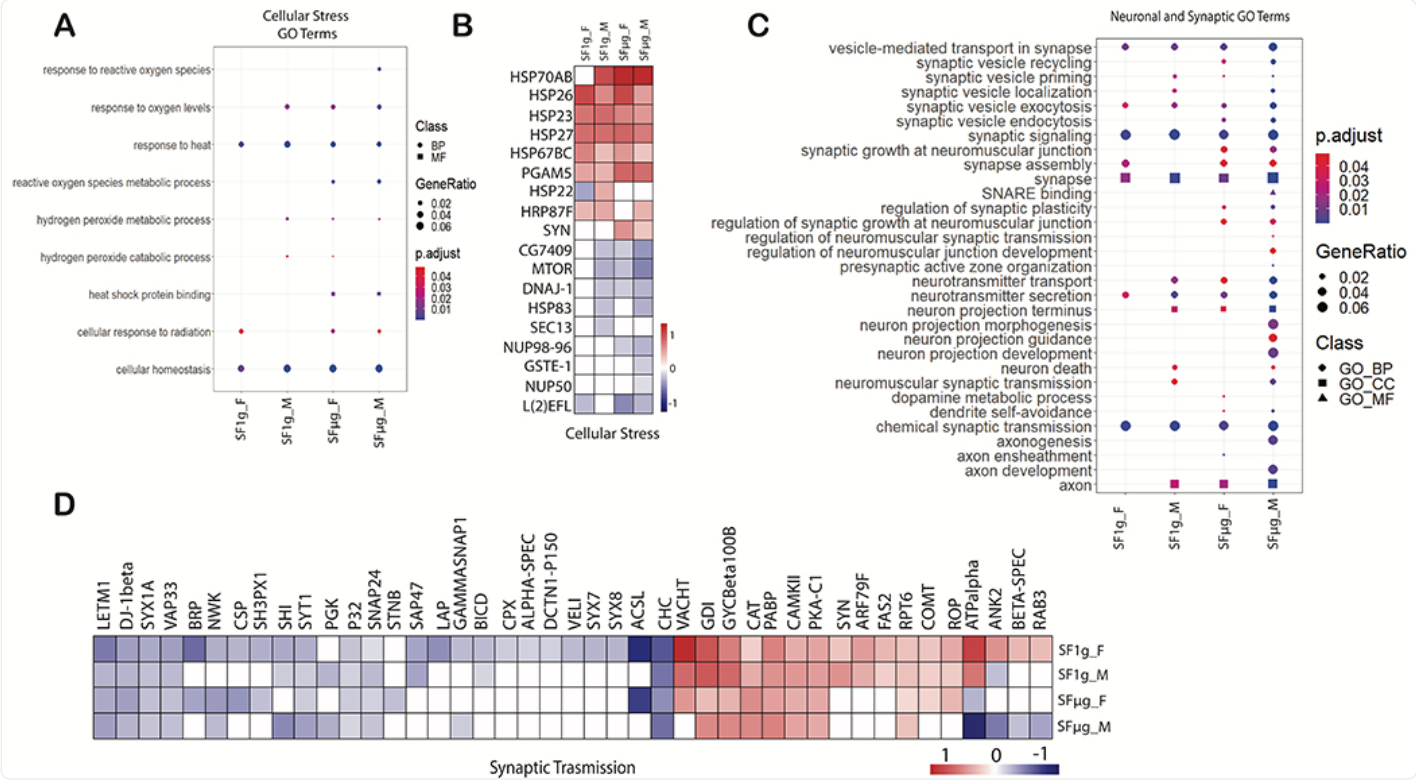

Open in a new tab

(A) Dot plot showing enriched GO terms (adj. p-value<0.05) associated with cellular stress in biological processes and molecular function for SF1g and SFµg (DEPs) compared to Earth. (B) Heatmap representation of differential expression (log2[fold-change]) of significantly altered (adj. p-value<0.05) cellular stress response proteins. (C) Dot plot highlighting enriched GO terms (p<0.05) associated with neuronal and synaptic signaling in biological processes, molecular function, and cellular components across all conditions (DEPs). (D) Heatmap displays log2[fold-change of proteins that are significantly altered (adj. p-value<0.05) in synaptic transmission. For dot plot, the color of the dot represents adj. p-value, and the size represents gene ratio. For heatmap, the red color represents upregulated and blue shows downregulated proteins.

In terms of neuronal functioning, we observed modulations in proteins involved in synaptic transmission across all spaceflight conditions (Figure 5D). For instance, SNARE protein syntaxin 1A (SYX1A), syntaxin binding protein SNAP24, presynaptic calcium sensor synaptotagmin (SYT), presynaptic calcium signaling protein P32, endocytic fission protein dynamin (SHI), and endocytic coat protein clathrin heavy chain (CHC) are downregulated. Meanwhile, the vesicle-mediated transport protein GDI, NSF1 protein that aids in disassembly of SNARE complex (COMT), cell-

cell adhesion mediator protein FAS2, vesicular trafficking protein ARF79F, and synapsin (SYN), a phosphoprotein associated with synaptic vesicles, among others are upregulated. These proteins collectively encompass almost every step of the synaptic vesicle cycle. The number of proteins altered is higher in SFµg condition than SF1g, and within SFµg condition, males show more changes than females, further reinforcing the selective sensitivity towards males and a dose-dependent response across spaceflight condition. Additionally, proteins associated with muscle and cytoskeleton are also noted in spaceflight flies (SFµg> SF1g) (Figure S5 C,D), consistent with previous spaceflight findings (Ogneva et al., 2016; Walls et al., 2020).

Persistent effects of exposure to spaceflight

Proteomics analysis suggests enrichment of behavioral and aging markers in SF1g and SFµg flies (Figure S6A). Specifically, the upregulation of HSP26, HSP27, HSP68, MTPalpha, CAT, SM, and TRXR-1, LDH, and downregulation of DJ-1beta, MSRA, and LEVY is observed across all conditions (Figure S6B). These proteins are also associated with oxidative stress response, which has been shown to increase with age (Lavara-Culebras and Paricio, 2007; Liao et al., 2008; Long et al., 2020a; Ren et al., 2017). To further understand the effects of spaceflight as the flies acclimate to Earth's gravity, we aged the flies for 25 days post-return under terrestrial conditions (R+25 days). Figure S7 shows the observed changes at R+25 timepoint for DA neuron counts, neuronal cortex area, apoptosis, and glial phenotypes. Overall, at the R+25 timepoint, the brain morphology of SF1g and SFµg is altered compared to Earth controls with sex-specific changes observed in the neuronal cortex area (Figure S7). We then performed the longitudinal comparison of morphological changes in fly brains between the R+0 (11-17 days old) and R+25 (36-42 days old) time points. This paradigm is similar to the post-mission evaluation of astronauts as they acclimate to Earth conditions over a period of time. Significant reduction of DA neurons was observed early in SFµg flies at the R+0 time point, compared to the gradual loss of these neurons in Earth and SF1g flies at the R+25 time point (Figure 6A). Typically, terrestrial conditions have not been associated with age-related loss of DA neurons (White et al., 2010), however, the elevated levels of CO_2 in Earth flies (analogous to SF1g and SFµg) in this study may contribute to the observed loss of DA neurons as the flies age in the Earth controls. Further, comparison of neuronal cortex areas between R+0 and R+25 data showed no change in the Earth flies, while decreasing trend over time was noted in SF1g flies and a significant reduction in SFµg flies, thus suggesting increased neuronal loss with age in space reared flies (Figure 6B). This loss correlates with increased apoptosis observed in R+25 flies, both SF1g (39%) and SFµg (70%) compared to R+25 Earth flies (Figure 6C). This progressive increase in apoptosis in space-reared flies (R+25 Earth < R+25 SF1g <R+25 SFµg) may suggest a dose-dependent response in flies as we move from Earth to space conditions with exposure to multiple stressors, including increased ionizing radiation combined with exposure to reduced gravity.

Figure 6: Persistent effects of spaceflight.

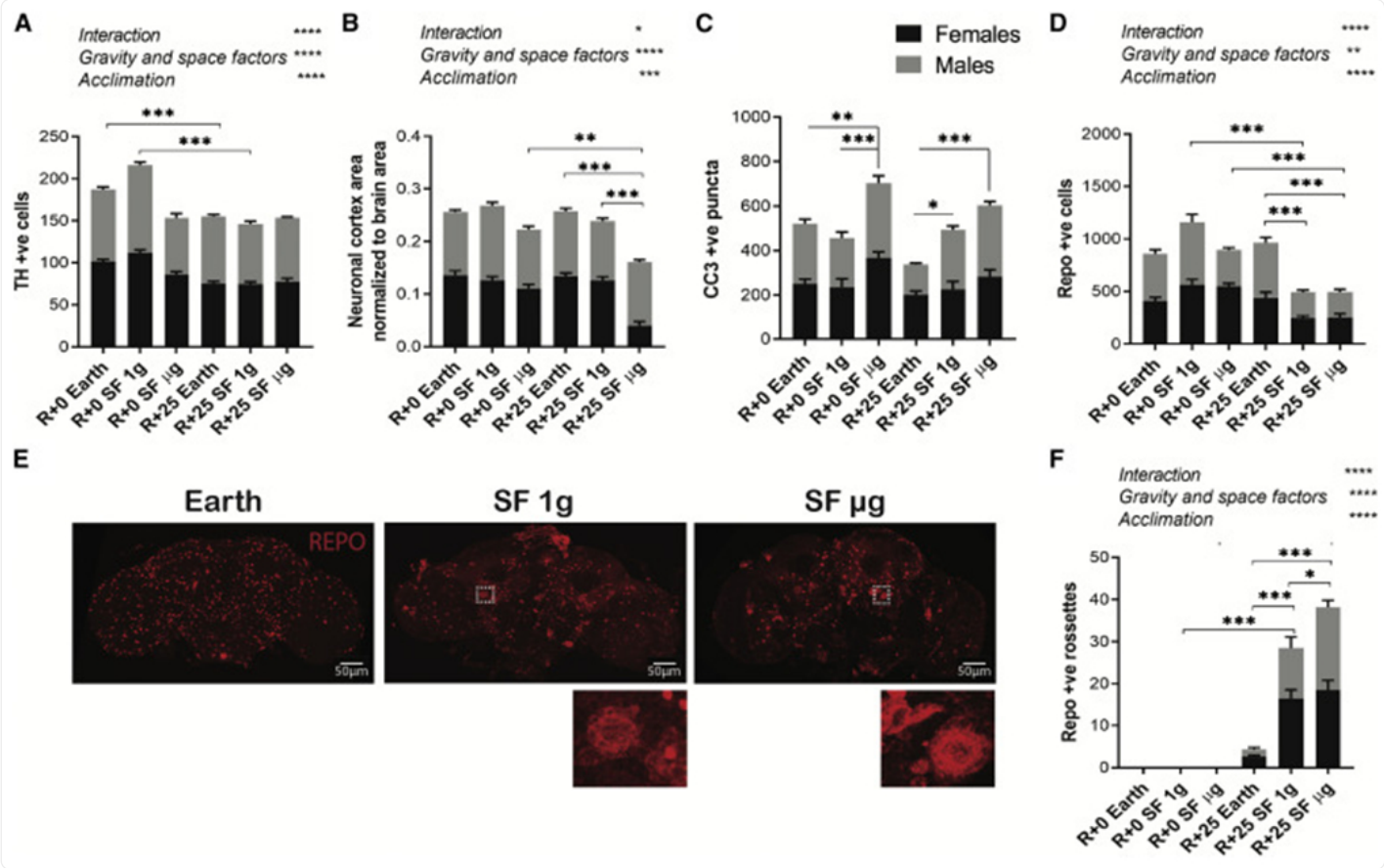

Open in a new tab

(A-D) Stacked bar plots showing quantification of DA neurons (A) (n=5-10), neuronal cortex area (B) (n=10-14), apoptosis (C) (n=5-7), and glia (D) at R+0 and R+25 days. (E) Representative images of R+25 fly brains labeled with anti-REPO (red). Quantification of Repo positive cells at R+25 days showed total glial loss (D) and increase in the aggregates/rosettes (F) (white box in E inset) in SFµg, SF1g (n=6-9). Two-way ANOVA results are displayed above the stacked bar plots. Significance calculated by post-hoc test is represented as *p<0.05; **p<0.01; *** p<0.001.

Additionally, we assessed glia, the primary phagocytic cell in CNS that are required to clear oxidative stress-induced neuronal debris (Bilimoria and Stevens, 2015; Casano and Peri, 2015; Cronk and Kipnis, 2013; Cunningham, 2013; Freeman, 2006; Hanisch and Kettenmann, 2007). At R+25, while we observe a slight but non-significant increase in glial cell numbers under Earth conditions (females: 7%, males: 17%), a significant depletion of the glial population in Earth acclimated SF1g (females: 56%, males: 59%), and sex-specific depletion in SFµg flies (females: 54%, males:

33%) is noted compared to their respective R+0 timepoint (Figure 6D, E). This depletion of the glial population can be due to burdening of the clearance system, eventually leading to glial apoptosis (Block et al., 2007), but additional investigation is warranted. Furthermore, as the flies age, we observe aggregates of glial cells that resemble rosettes (Figure 6E, inset). These rosettes were distinct in size and appearance from other glial cells and were not counted towards total repo-positive cell counts (Figure 6D); instead, they were counted separately (Figure 6F). This rosette phenotype is absent at the R+0 time point in all conditions, whereas it is observed at the R+25 time point specifically after exposure to spaceflight-related stressors in a dose-dependent manner (R+25 Earth < R+25 SF1g <R+25 SFμg) (Figure 6F). We believe the rosette to be a phenotype manifested as a long-term effect of the spaceflight environment. The rosette formation could result from factors such as elevated CO_2 levels and can be exacerbated by the combinatorial effect of other spaceflight stressors such as ionizing radiation and reduced gravity.

While some of the immunohistochemical and omics results described here resemble early aging, more assays at additional time points need to be performed for further validation of the effect of spaceflight on related aging phenotypes. Although omics profiling at the R+25 time point would be informative and will be considered in future missions, these experiments were not feasible here since the flies were distributed for the other assays reported above. Taken together, the brain morphology at R+0 time point is similar in SF1g and Earth conditions, but as the flies age postflight under terrestrial conditions, the morphological deficits start manifesting in SF1g flies and are worsened over time in SFμg, suggesting a phenotype that is manifested after exposure to spaceflight.

Discussion

Deep space exploration will expose space travelers to several environmental challenges, thereby altering the homeostatic equilibrium of various physiological systems, including the CNS. Understanding the risks to CNS and identifying countermeasures to mitigate these risks in astronauts will be crucial to ensure the success of missions to the Moon and Mars. Using MVP, a fruit fly space habitat, we provide insights into spaceflight effects on the brain at the molecular, morphological, and behavioral levels. While AG by rotation of the spacecraft is being considered as a potential countermeasure to μg, there is a gap in our understanding of AG prescriptions required to ameliorate the health concerns during spaceflight (Clément, 2017; Clément and Traon, 2004; Mao et al., 2018a; Young, 1999). To address this knowledge gap, we utilized the MVP hardware featuring an inflight centrifuge that simulates Earth's gravity on the ISS (SF1g). SF1g served two objectives: 1) assessment of the use of AG as a countermeasure; and 2) distinguishing the effects of μg from other spaceflight stressors, such as radiation.

A key feature of the MVP hardware, the inflight video recording capability, aided in assessing the health of the flies during the mission and provided real-time data of behavioral alterations caused by the change in the gravitational environment. Due to the large number of videos taken on the mission, manual analysis by visual assessment was not feasible, nor was the use of specialized equipment traditionally used to assess fly behavior in ground laboratories (Chan et al., 2012; Inan et al., 2009, 2011; Kohlhoff et al., 2011; Slawson et al., 2009). Also, the constraints in video quality,

such as uneven light distribution, inability to focus on flies in the foreground and the background, prevented the use of sophisticated tracking and machine learning algorithms for behavioral analysis. Therefore, a simple yet effective automated method was developed to quantitatively capture overall behavioral differences across spaceflight conditions. The overall level of activity of a population is a trait influenced by the environment and can be used to assess other physiological changes. Miller et al. suggested that fly hyperactivity in µg is a result of their innate negative geotactic response (Miller et al., 2002). Interestingly, our findings follow a similar trend, apart from the population flux point (day 20), we consistently observed that flies in SFµg are more active than those in SF1g (Figure 1D, E). This data suggests that AG may suppress the hyperactive behavior in flies during spaceflight.

Similar increases in fly activity (Benguría et al., 1996) and mouse circling behavior (Ronca et al., 2019) in spaceflight conditions have been reported. Future improvements in the flight hardware might aid in quantifying individual fly activity, thus providing further insights into behavioral changes caused by gravity changes and the ability to test the effectiveness of countermeasures.

A substantial fraction of the literature on the CNS effects of spaceflight focuses on either anatomical changes or molecular changes using omics platforms. In this study, we took a multimodal approach combining the morphological analysis with the omics-based molecular phenotyping for a comprehensive understanding of the underlying mechanisms associated with spaceflight-induced brain changes. At the transcriptomics level, we observed a higher number of differentially regulated genes in SFµg compared to Earth, specifically in females. Meanwhile, the SF1g females show fewer changes in RNA compared to Earth (Figure 3). Interestingly, at the proteomic level, the number of DEPs is relatively similar and show considerable overlap across spaceflight conditions (SF1g vs Earth and SFµg vs Earth). In many studies a discordance is observed between the two omics platforms; nevertheless, each data set offers unique insights into spaceflight-associated changes (Casas-Vila et al., 2017; De Sousa Abreu et al., 2009). While transcriptomic analyses provide broad-scale insights into molecular dynamics that occur on the level of mRNA regulation, most physiological processes are driven by protein function. Based on proteomics one important theme that was captured across both spaceflight conditions was a change in metabolic pathways, including oxidative phosphorylation (Figures 3–5). These are consistent with previously published data on space-flown human kidney cells (Hammond et al., 2000) and mouse brain subjected to spaceflight (Mao et al., 2018b).

The brain is a metabolically dynamic and high-energy-demanding organ that is dependent on mitochondria for deriving energy *via* various metabolic processes that converge at glycolysis and oxidative phosphorylation (Hall et al., 2012; Magistretti and Allaman, 2015). Normal functioning of the brain requires a tight temporal and spatial regulation of metabolite supply for energy production (Roy and Sherrington, 1890; Watts et al., 2018). We observe such metabolic regulation in spaceflight flies with increased glucose, fatty acid, and amino acid metabolism (Figure 4E, H, I). Additionally, spaceflight flies exhibit alteration in proteins of the electron transport chain (ETC) and ATP metabolism (Figure 4F, G), similar to the observations in mice, astronauts, and the NASA Twins Study (da Silveira et al., 2020). Such dysregulation of ETC and abnormal mitochondrial dynamics (Figure 4D) can lead to mitochondrial and oxidative

stress *via* ROS production (Bhatti et al., 2017). Oxidative stress during spaceflight is further evidenced by an increase in 8-oxo-dG, cellular oxidative stress marker, in the SFµg fly brain at R+0 time point (Figure 2E, I), and is consistent with the increase of 8-oxo-dG in urine and plasma samples in astronauts (Rai et al., 2011; da Silveira et al., 2020). On the contrary, SF1g brains at the R+0 time point showed no significant change in the 8-oxo-dG marker, thus suggesting that AG can suppress oxidative damage in the brain immediately after return from spaceflight (Figure 2E, I).

We hypothesize that the observed alterations in the metabolic pathways are an effort to restore cellular homeostasis *via* metabolic reprogramming. While homeostasis is restored in R+0 SF1g, possibly due to AG, as evidenced by their similar brain morphology to Earth flies (Figure 2), microgravity in SFµg acts as an additional stressor, potentially resulting in elevated oxidative stress. This stress can further trigger a cascade of events leading to neuronal damage as noted in the behavioral deficits (Figure 2A), loss of DA neurons (Figure 2E, F), decreased neuronal cortex and neuropil areas (Figure 2B–D and Figure S3B), and increased apoptosis (Figure 2E, H) in SFµg flies. Additionally, we observe perturbations in synaptic transmission proteins during spaceflight (Figure 5C, D), which in combination with bioenergetic changes (Figure 4) can result in dysregulation of calcium homeostasis and synaptic degeneration (Mattson and Liu, 2002). Synaptic changes have also been documented in multiple spaceflight and ground-based rodent studies (Bondar, 2005; DeFelipe et al., 2002; Gaofei et al., 2009; Howe et al., 2019; Machida et al., 2010; Mao et al., 2018; Parihar et al., 2015, 2016; Ranjan et al., 2014; Ross and Varelas, 2005; Sokolova et al., 2015; Wang et al., 2015). Neuronal damage and loss induced by elevated oxidative stress can potentially alter the glial response, initiating phagocytosis to clear neuronal debris (Block et al., 2007). While our observations of glial numbers immediately after return (R+0) shows an increasing trend in SFµg females and SF1g (females and males) (Figure 2G), further analysis is warranted to elucidate the underlying mechanism of change in glial function. Collectively, our observations suggest that brain morphological changes due to spaceflightinduced oxidative stress are more pronounced in µg conditions, and AG can provide partial protection to these phenotypes.

Based on our omics data, R+0 morphology, and the radiation levels on ISS, gravity seems to have a significant impact on the immediate phenotypes of spaceflight with larger observable changes in SFµg compared to SF1g. The environment experienced by the flies in SFµg compared to SF1g allows the comparison of gravity separately from the combined effect of the other spaceflight stressors like radiation, elevated CO_2, and sound pressure which would equally impact both SF1g and SFµg. Although the morphological manifestations are not observed in SF1g flies at R+0 time point, with age (R+25), the phenotypes progressively present themselves in the form of increased apoptosis, neuronal loss, glial loss and aggregate formation (Figure 6AF). Glial loss may be attributed to the relocation of glia to the neuronal debris, thus resulting in aggregates (formation of rosettes), a phenotype specific to the spaceflight environment. These phenotypes in SF1g at R+25 may be a delayed response to radiation combined with exposure to other space stressors such as elevated CO_2. Radiation studies in ground-based rodent models indicate that exposure to deep space radiation (galactic cosmic radiation or GCR) alone can affect behavior (Dutta et al., 2018; Euston et al., 2012; Parihar et al., 2015, 2018; Raber et al., 2018b), and neuronal phenotypes (Davis et al., 2015; Howe et al., 2019; Impey et al., 2016; Krukowski et al., 2018; Parihar et al., 2015, 2016; Raber et al., 2016, 2018b, 2019; Rabin et al.,

2014; Whoolery et al., 2017). In an enclosed and isolated environment of the ISS, astronauts experience elevated CO_2 levels that are considerably higher than ambient levels on Earth (Mahadevan et al., 2021). In our study, the Earth control flies were exposed to an environment mimicking ISS and experienced high CO_2 levels similar to SF1g and SFμg flies, in contrast to regular lab conditions. Mild chronic hypercapnia due to constant exposure of elevated CO_2 levels may contribute to the observed deficits of decreased TH positive cells, and repo positive rosettes (<10) in the Earth control flies at R+25, along with the increased cell death (CC3 positive cells) and DNA oxidation (8-oxo-dG positive cells) as noted at R+0 in Earth controls. In fact, in our ground-based study, we observed minimal cell death and DNA oxidation under normal terrestrial CO_2 levels compared to Earth control brains from the MVP mission exposed to elevated CO_2 levels (data not shown). Thus, the observations reported in the Earth controls are part of the unique spaceflight paradigm and may not be comparable to controls in terrestrial studies. While ground studies are important in separating the effects of individual space stressors, spaceflight studies are particularly relevant as we prepare for long-duration human missions to the Moon and Mars where there will be a combination of exposures to reduced gravity and doses of ionizing radiation that will be higher than in LEO (Mao et al., 2017; Straume et al., 2017).

This study integrates transcriptomic, proteomic, morphological, and behavioral analyses to investigate the effects of spaceflight on *Drosophila* CNS both during and after return from spaceflight. Further, our study utilizes inflight centrifuge mimicking Earth 1g, as a control that allowed us to separate μg from the effects of other spaceflight environmental factors such as ionizing radiation. Additionally, the postflight acclimation to Earth's conditions is relevant to understanding the sustained effects of spaceflight on the CNS. Our integrated approach suggests that oxidative stress during spaceflight leads to differential regulation of metabolic pathways, oxidative phosphorylation, and synaptic transmission resulting in neuronal deficits, glial changes, increased apoptosis, and behavioral impairments in *Drosophila*. Furthermore, this study indicates that μg is an important but not an exclusive environmental factor contributing to the neurobehavioral outcomes during long-term deep space missions. AG may provide a measure for short-term protection, but long-term solutions still need to be explored, especially for longduration missions in deep space. Earth's magnetosphere partially protects against ionizing radiation from GCRs and solar particle events (SPE) in LEO, but beyond LEO, deep space irradiation will pose significant risks to crewmember health. Thus, along with AG, future countermeasure studies should target these pathways in model organisms that are amenable to large-scale screening in space.

Limitations of the study:

The opportunity to conduct spaceflight experiments is not only rare and expensive, but the logistical constraints of such studies also make them highly challenging to perform (Inokuchi et al., 2007; Rutter et al., 2020). For instance, the experiment launch and retrieval can be significantly altered due to weather or technical issues with the spacecraft, thus necessitating a flexible experimental design to achieve the intended science goals. In fact, our sample return was delayed from 31 days to 34 days due to weather-related issues. Another constraint of spaceflight studies is that retrieving exact age-matched flies is often not feasible. Some of the previous spaceflight studies have been conducted on

mixed-age populations of flies from different generations (depending on the mission's timeline). But with the MVP hardware, the astronauts could accommodate multiple timed inflight operations, including a 5.5-day egglay period (Figure S1C), thus ensuring that the retrieved flies were from the same generation and within a relatively close age range (11-17 days). Our strategy of testing randomly selected flies from this collection ensured that the average ages were similar and allowed for an unbiased comparison across groups of flies. Further, spaceflight experiments are severely limited by mass and volume. Therefore, the number of samples retrieved is limited by the capacity of the flight hardware. In this experiment, a large population of live flies were retrieved from the MVP hardware, allowing us to conduct the presented experiments. Additional flies would have allowed for longitudinal multi-omic profiling at the R+25 time point but were unavailable for this experiment. The current study, MVP-FLY-01 mission, was an important one-time validation flight for the MVP hardware to demonstrate its ability to support *Drosophila* research on the ISS. After its successful validation, as demonstrated by this experiment, this hardware will form the framework for multiple *Drosophila* spaceflight investigations in the future.

STAR Methods

RESOURCE AVAILABILITY

Lead Contact

Further information and requests for resources should be directed to and will be fulfilled by the lead contact, Sharmila Bhattacharya (sharmila.bhattacharya@nasa.gov).

Materials availability

This study did not generate new unique reagents.

Data and Code availability

- All data reported in this paper will be shared by the lead contact upon request. Transcriptomic and proteomic data (Raw read counts and FASTQ files) are made available at the community-endorsed public repository at NASA Gene Lab.
  The code generated during this study is openly available on GitHub at https://github.com/Siddhitamhatre/MVP-inflight-behavior
- Any additional information required to reanalyze the data reported in this paper is available from the Lead Contact upon request.

EXPERIMENTAL MODEL AND SUBJECT DETAILS

A. Spaceflight mission and Hardware Description

The MVP-Fly01 mission (Figure 1A, B) was launched on SpaceX-14 to the ISS at 20:30 UTC (Coordinated Universal Time) on April 2nd, 2018. Flies were kept in the MVP hardware throughout the 34-day mission on the ISS (Figure S1A). The Dragon capsule was unberthed at 13:22 UTC on May 5th, 2018, and splashdown in the Pacific Ocean was the same day at 20:00 UTC. The mission used the MVP hardware (Redwire/Techshot, Inc., Greenville, Indiana) that supports easy food changes, allowing for a large population of flies to be maintained over multiple generations. It is also equipped with UI-1491LE video cameras used to capture time course footage of *D. melanogaster* (Figure S1B). The hardware consists of uniform white LED illumination which was programmed for a 12-hr:12-hr (light: dark) cycle for each habitat. Fresh cabin air was continuously circulated through the habitat to maintain steady CO_2 and O_2 levels. The housing system consists of two independent centrifuge units maintained within the same habitat enclosure, each containing six MVP modules (Figure S1A, B). For this experiment, one centrifuge was rotated at 68 rpm to artificially simulate Earth's gravity (SF1g) in space. The other centrifuge was rotated at 2.2 rpm, making the g-level at the outer edge of the carousel at approximately 0.00095g (SFμg). This minimal rotation of SFμg ensured temperature uniformity between all experimental modules, while maintaining the microgravity levels of the ISS. Each MVP module has two adult fly chambers and three food cylinders (Figure S1B). Each food cylinder holds approximately 9.2 mL of standard fly food (Gilbert et al., 2020) containing foodgrade blue food dye. The presence of the dye allowed for the differentiation between early and late third instar larvae during postflight specimen sorting. Its inclusion is not relevant to the current analysis of adult flies performed here. The hardware design allowed for the passage of two generations of flies sequentially from adult fly chamber 2 to adult fly chamber 1 (Figure S1B). The MVP hardware has video imaging capabilities, and 28-second video footage of the adult fly chambers was taken regularly throughout the 12-hr light period. Although the MVP hardware has night video recording capability, it was not utilized in this mission due to technical difficulties with the infrared lighting.

Each 28-second video consisted of 368 frames with an image resolution of 1986×1064 pixels. This video was periodically checked during the mission to ensure the health of flies and gauge the overall well-being. Upon return, this video was analyzed for inflight behavior to compute adult fly activity in SF1g and SFμg conditions during the mission. Following the completion of the mission, the samples were returned to Port of Long Beach, California, and transported *via* a climate-controlled vehicle to NASA Ames Research Center (ARC), California, within 7 hours of landing. Temperature and humidity loggers were also programmed to monitor the samples throughout the journey. All dissections, fixation of brain tissue, and postflight behavioral analysis (described below) were performed within 24 hours of arrival at NASA ARC (Return+0 days = R+0). A small subset of flies separated by sex was placed in an incubator at 24°C for acclimation to earth condition for 25 days (Return+25 days = R+25), and the brains from these flies were processed for immunohistochemical analysis similar to R+0 flies (Figure 1B).

During the mission, a small set consisting of only two MVP modules (synchronous control) was reared in a ground-based incubator with real-time changes in temperature, humidity, and CO_2 matching the telemetry recorded on the ISS. The synchronous control was checked periodically to ensure the overall health of the flies during the mission but was not used for any of the postflight analysis. Upon completing the mission, a postflight ground control with the same hardware used for the mission was conducted in a ground-based incubator with six MVP modules resulting in 883 flies. For the postflight control (Earth), flies were placed in each module to match the flight condition and were reared under identical conditions to match the temperature, relative humidity, O_2, and CO_2 levels recorded for the entire experiment on the ISS. The CO_2 levels within habitats in space are often significantly higher than those on the ground due to the technical difficulty of scrubbing the CO_2 from an entirely enclosed environment (ISS). The average CO_2 level in the MVP hardware during this experiment ranged between 3500-5443 ppm during the mission and was replicated temporally and identically in the ground control. By comparison, the CO_2 level under regular laboratory conditions averages <1000 ppm (Hussin et al., 2017). Also, another variable in any spaceflight study is sound pressure level. Based on ISS's telemetry data and payload permissible limits, SF1g and SFμg flies in the MVP module on ISS experienced average sound pressure levels of 65dB. Similar sound pressure levels (62-65dB) were noted in the vicinity of the Earth controls placed in the laboratory incubator (Percival Scientific). The Earth control flies were fixed in RNAlater and subjected to postflight analyses following the same timeline as the flies from ISS. The Earth control used for comparison and statistical analysis in this manuscript is this postflight ground control.

B. Fly husbandry, loading the module, and development

The w^{1118} wildtype line (Bloomington Stock Center) was used in this study. Thirty hours prior to launch, one-day-old virgin male (10) and female (25) fruit flies were loaded into the adult food cylinder 3 in each of the six MVP modules (F0 generation). The food cylinder was then immediately opened to adult fly chamber 2 (Figure S1B, C). The modules were then placed inside of a standard cargo transfer bag for launch. Prepared food cylinders were stored at 4°C for the duration of launch and ISS operations. Approximately 3.7 days (90 hrs) after launch, the payload was delivered to the ISS and the crew installed a food cylinder 2 inside the MVP module and opened the food cylinder 2 to adult fly chamber 2 (Mission day=5), giving flies access to the new food. Food cylinder 3 was closed at this time. This procedure was repeated for all MVP modules, and the modules were loaded into the previously installed MVP habitat hardware (Figure S1A) by the ISS crew. At this time, the six SF1g modules started spinning at 68 rpm to maintain 1g in spaceflight while the six SFμg modules were maintained at microgravity levels.

After 5.5 days of egg laying (Mission Day=10), food cylinder 2 was opened to adult fly chamber 1 to allow the eggs laid in space to develop and emerge into adult flies in chamber 1. At the same time food cylinder 2 was closed to adult fly chamber 2, such that the launch populations of flies were prevented from entering food cylinder 2, thus keeping the generations separated (Figure S1C). Food cylinder 3 was reopened to adult fly chamber 2 to continue providing food to this population for the remainder of the experiment. The larvae and flies that emerged from the food cylinder 2 into the adult fly chamber 1 had undergone their entire developmental life cycle during spaceflight (F1 generation). At this time,

food cylinder 1 was inserted and opened to chamber 1 to allow egg laying in cylinder 1, which will produce the second generation of spaceflight-developed flies (F2 generation). Food cylinder 2 remained open to chamber 1 during egg lay to allow adults to continue emerging. This also allowed us to know the age range of the adult flies returned for postflight experiments (~11-17-day adults).

After 8 days of egg laying, food cylinder 1 from each module containing F2 generation fruit fly eggs and larvae, and some F1 generation adults, was fixed in RNAlater (Invitrogen).

This allowed us to have samples that were fixed in RNAlater in space for "omics" analyses on the ground to track the progression of acclimation to spaceflight as animals develop in space under different gravity conditions. Following the fixation, a fresh food cylinder 1 was inserted and opened to chamber 1, and food cylinder 2 was closed. The MVP locker was powered down after the experiment, and fixed F1 generation flies and F2 generation eggs and larvae were placed in the MELFI-2 freezer at −80°C until the samples returned. Thus, this experimental design allowed us to freeze adult flies (F1 generation), larvae (F2 generation), and eggs (F2 generation) at Day 29. Postflight, we retrieved live adult flies (F1 generation), and eggs and larvae of F2 generation in the new food cylinder 1. All the science operations, including food cylinder changes and fixation and opening/closing of chambers, were performed by the ISS crew. Unforeseen weather conditions delayed the mission by 4 days, during which the crew repowered the MVP hardware on mission day 31 and powered it off on mission day 34 for return to Earth.

METHOD DETAILS

A. Inflight behavioral analysis

To quantify fly activity on the ISS, a simple but robust algorithm was developed using image-processing techniques in Matlab 2018 (MathWorks, Inc., Natick, MA) and DIPimage (Hendriks et al. 1999) running on a MacBook Pro with an i7 core processor. Only the videos from adult fly chamber 1 SF1g and SFμg were analyzed in this study (Mission days 13 to 28 – Figure S1C) since these chambers contained the flies bred entirely in space (F1 generation). The age of the flies assessed from video imaging of the inflight behavior ranged from 1 to 16-days (Postflight assays were conducted with flies with a smaller age range as described in the relevant sections). Similar video recording arrangements were made for Earth condition, but the videos could not be recorded due to technical issues. Full resolution 8-bit images (1986x1064) were used for analysis. The individual frames from the video images have a predominant intensity in the blue channel (Figure 1C.i). Therefore, each video image was separated into its three RGB components, and the blue channel (shown in grayscale) was inverted and used for further analysis (Figure 1C.ii) as it provided best visualization of the flies. Once inverted, resulting images had individual flies that appeared as white pixels on a gray background. For each movie, maximum intensity projections (MIP) were computed by overlaying individual video frames and keeping the brightest pixels across all time points, resulting in a stroboscopic motion-like effect (Figure 1C.iii and 1C.iv). The

pixel location of the MIP was mapped on a composite image to visualize the locomotion of individual flies during each video. These tracks had a higher intensity and appeared brighter than the background. Flies that did not move did not create a track, as seen between Figure 1C.ii and 1C.iii indicated in green. However, flies that were active during the video recording created a white track, shown in Figures 1C.ii and 1C.iii in blue and red. This process resulted in a single image that displayed the tracks of the fly population throughout a series of 28-second video recordings (Figure 1C.iv).

Using the MIP images of adult fly chamber 1, we could determine when flies were active. The videos from mission day 13 to 28 (Figure S1C) that tracked the F1 generation of flies as shown in Figures 1D, E. In other words, this time frame included initial fly emergence when the majority of the space-bred generation of flies entered adult fly chamber 1 from food cylinder 2 but ended prior to fly numbers and debris levels increasing to a point where the camera view was obstructed (Figure S2). The number of flies in a chamber increased over time due to reproduction based on the life cycle of *D. melanogaster* (Fernández-Moreno et al., 2007) (Figure S2). Six videos per day, each 28 seconds in duration that spanned the 12-hr light period, were processed to produce MIP images for each fly module. One of the six modules containing the population bred in µg malfunctioned during flight, so our analysis includes six modules in SF1g and five modules in SFµg. Videos from adult fly chamber 2 were not used for analysis because 1) the build-up of debris due to more extended periods of growth compared to adult fly chamber 1 obscured the camera view, and 2) the chamber contained mixed generations of flies. The pixel intensities were summed for each MIP image, resulting in a single numerical value for every video. The more a fly moves, the longer are the white streaks that can be observed along its path on the MIP and the higher is the total measured intensity. The process was repeated for each video producing a series of numerical values to quantify the overall activity of the fly population during the mission. Supplementary video 1, 2 is a representative video showing the fly chambers of SF1g and SFµg, where suspended flies are seen in microgravity condition. The color map in Figure 1D was generated by setting the minimum value in the color map to the baseline intensity obtained from the first frame of the video. The intensities across all modules and treatments were scaled such that the video with the MIP image having the highest summated intensity (and therefore highest activity) was set to the maximum color on the color scale (Figure 1D). Note: No videos were analyzed for activity past day 28 due to the increased fly numbers and debris interfering with the image quality.

B. Climbing assay

Climbing assay was performed on F1 generation of flies returned to Earth using a modified version of Le Bourg and Lints (Feany and Bender, 2000). For each condition, flies were sorted and collected by sex, in groups of ten per food vial (F=100, M=100) as soon as the live flight samples were returned on earth (i.e., Fig. 1B, splash at L+34, 2 days for samples turnover (Long Beach, CA) and arrived at NASA ARC (R+0) and the assay was conducted.

During the climbing assay, flies were transferred to a clean, empty vial and allowed to adjust for 1 minute. The flies were tapped down to the bottom, and the number of flies climbing past the 5 cm mark measured from the bottom of the vial in 18 seconds was recorded as a percentage of flies able to climb per vial (climbing ability). This assay was

repeated three times for each vial, with a 30 second rest between trials. An average of three trials was reported per vial.

Measurements from all three trials were averaged. The significance was determined between the conditions by a one-way ANOVA analysis with the condition as the independent variable.

C. Immunohistochemistry and confocal imaging of brains

F1 generation flies returned live were dissected (R+0 and R+25) and brains were immediately fixed for 20 minutes in PBS (Phosphate buffered saline) containing 4% paraformaldehyde, 6.7% sucrose, and 0.01% tween-20, and stored at 4°C in PBS with 0.05% sodium azide. The R+0 and R+25 brains were stained for immunohistochemical analysis (described below) where staining for different antibody markers was conducted at the same time to facilitate comparison and reduce variability. The brains were stained following a standard protocol (Iyer et al., 2018; Mhatre et al., 2014). Briefly, the fixed brains were washed with PBS and PBT (0.2% Triton X-100 in PBS) for 10 min each, incubated with blocking buffer (5% normal goat serum (Catalog # 566380, Sigma) in PBT) for one hour, and then incubated overnight at 4°C with primary antibodies. One set of brains were stained with anti-elav (1:100, Catalog # 7E8A10, Developmental Studies Hybridoma Bank (DSHB), host species - rat) to label all the neurons, anti-cc3 (1:100, Catalog # 9661, Cell signaling Technology, host species - rabbit) as apoptotic marker, and anti-8-oxo-dG (1:100, Catalog # 4354-MC-050, R&D systems, host species - mouse) as the DNA oxidative damage marker. Another set of brains were stained with anti-Repo (1:50, Catalog # 8D12, DSHB), University of Iowa, host species - mouse) to label the glia, and anti-TH (1:300, Catalog # AB152, EMD Millipore, host species - rabbit) to label the dopaminergic neurons. These preparations were then washed three times with PBT for 10 min each, and incubated with fluorophore-conjugated secondary antibodies, Alexa fluor 568 goat anti-mouse (1:200; Catalog # A-11031, Invitrogen), Alexa fluor 488 goat anti-rabbit (1:200; Catalog # A-11034, Invitrogen), or Alexa fluor 633 goat anti-rat (1:200; Catalog # A21094, Invitrogen). Final washes were performed once with PBT and twice with PBS, each for 10 min, and mounted in Vectashield (Vector Labs, H-1000) for imaging.

Stained brains were imaged using Zeiss LSM 880 laser scanning confocal microscope in the histology and microscopy core facility at the Gladstone Institute, University of California San Francisco (UCSF). The ELAV neuronal cortex, neuropil, and the total brain area were traced and quantified using Image J software (v1.52g, U. S. National Institutes of Health, Bethesda, Maryland, USA). This method is a gross measurement adapted from previously published papers (Chakraborty et al., 2011; Mhatre et al., 2014). The data reported here are the neuronal cortex and neuropil area normalized to the total brain area. Similarly, the number of puncta for TH (total number of TH-positive cells), repo, 8-oxo-dG, and CC3 were analyzed and quantified for each stain/marker using the cell counter in ImageJ software and are reported as absolute values.

D. RNA isolation, sequencing, and analysis of fly heads

The food cylinders that were frozen on ISS were slow-thawed at 4°C before opening. Once thawed, cylinders were opened, and flies (F1 generation frozen at L+29 days) were removed and sorted by sex. The head was removed using spring scissors and placed in RNAlater to preserve the RNA and protein integrity. Total RNA was extracted using RNA/ Protein Purification plus (Norgen) from adult heads with four biological replicates in each condition (12-15 heads per replicate). This kit isolated total RNA and protein from the same samples. Isolated RNA was used to perform paired-end RNA sequencing on Illumina Novaseq 6000 platform, with an average of 20M reads of PE150 per sample (Novogene, Sacramento, CA). Data validation and quality control with FASTQC were conducted by Novogene, Inc. The standardized Genelab pipeline was used for the analysis (Overbey et al., 2021). Briefly, raw RNA sequences were trimmed using Trim Galore! v0.6.2 (Krueger, 2019), aligned to the *Drosophila* reference genome (Dmel release 6.08) and transcriptome with STAR Version 2.7.1a (Dobin et al., 2013), and read counts for each transcript were generated using RSEM v1.3.1. Differentially expressed gene lists were generated using a custom Genelab R script, GeneLab_DGE_noERCC.R, utilizing the DESeq2 v1.22.2 R package (Lai Polo et al., 2020). False discovery rate (adjusted p-value) corrections were performed using Benjamini-Hochberg multiple testing adjustment, and the differentially expressed genes with an adjusted p-value of less than 0.05 were considered statistically significant.

E. Proteomics and analysis of fly heads

Proteins isolated from adult heads (F1 generation frozen at L+29 days) using the Norgen Biotek kit were used to determine the global proteomic changes. Three replicates in each condition (12-15 heads per replicate) were used for protein isolation and enzymatic digestion. Isolated protein samples were digested and desalted according to Lundby et al. (Lundby et al., 2012). Protein concentrations were then determined using a bicinchoninic acid assay (BCA) (Thermo-Fisher Scientific, San Jose, CA). Proteins were then reduced, alkylated and subjected to acetone precipitation prior to digestion with endoproteinase Lys-C, 1:50 enzyme to protein (Wako, Richmond, VA). This was followed by digestion with trypsin, 1:50 enzyme to protein (Promega, Madison, WI), and desalting and concentrating using C_{18} Sep-Pak cartridges (Waters).

TMT Isobaric Labeling -

Peptides were mass tagged using Thermo-Fisher's TMT 10-plex isobaric label kit (Catalog # 90061) following the included protocol and pooled for analysis. Six experimental conditions were labeled in triplicate across three TMT-runs, including two internal control channels.

Basic Reversed-Phase Fractionation –

Pooled TMT-labeled peptides were fractionated by basic pH reversed-phase (BPRP) fractionation on an Ultimate 3000 HPLC (Thermo Scientific) using an integrated fraction collector. Elution was performed using a 10-minute gradient of

0-20% solvent B followed by a 50-minute gradient of solvent B from 20-45% (Solvent A 5.0% Acetonitrile, 10mM ammonium bicarbonate pH 8.0, Solvent B 90.0% Acetonitrile, 10mM ammonium bicarbonate pH 8.0) on a Zorbax 300Extend-C18 column (Agilent) at a flow rate of 0.4 ml/min. A total of 24 fractions were collected at 37-second intervals in a looping fashion for 60 minutes then combined to produce 12 super fractions. Peptide elution was monitored at a wavelength of 220nm using a Dionex Ultimate 3000 variable wavelength detector (Thermo Scientific). Each fraction was then centrifuged to near dryness and desalted using C_{18} Sep-Pak Cartridges followed again by centrifugation to near dryness and reconstitution with 20 ul of 5% acetonitrile and 0.1% formic acid.

Liquid Chromatography and Mass Spectrometry-

BPRP fractions were then separated using an UltiMate 3000 RSLCnano system (Thermo Scientific, San Jose, CA) on a self-packed C18 column (100 um x 35 cm). Separation was performed using a 180-minute gradient of solvent B from 2-27% (Solvent A 0.1% Formic Acid, Solvent B Acetonitrile, 0.1% Formic Acid) at 50°C using a digital PicoView nanospray source (New Objectives, Woburn, MA) that was modified with a custom-built column heater and an ABIRD background suppressor (ESI Source Solutions, Woburn, MA). An in-house column was prepared by packing a 100µm inner diameter picofrit column (New Objectives, Woburn, MA) with 1.9µm ReproSil-Pure C18 (Dr. Maisch, Ammerbuch, Germany) and packed to a length of 30 cm at 9000 psi using a nano-LC column packing kit (nanoLCMS, Gold River, CA).

Mass spectral analysis was performed using an Orbitrap Fusion mass spectrometer (Thermo Scientific, San Jose, CA). TMT analysis was performed using an MS3 multi-notch approach. The MS1 precursor selection range is from 400-1400 m/z at a resolution of 120K and automatic gain control (AGC) target of 2.0×10^5 with a maximum injection time of 100 ms. Quadrupole isolation at 0.7 Th for MS^2 analysis using CID fragmentation in the linear ion trap with a collision energy of 35%. The AGC was set to 4.0×10^3 with a maximum injection time of 150ms. The instrument was operated in a top-speed data-dependent mode with a most intense precursor priority with dynamic exclusion set to an exclusion duration of 60 seconds with a 10ppm tolerance. MS2 fragment ions were captured in the MS3 precursor population. These MS3 precursors were then isolated within a 2.5 Da window and subjected to high energy collision-induced dissociation (HCD) with a collision energy of 55%. The ions were then detected in the Orbitrap at a resolution of 60,000 with an AGC of 5.0×10^4 and a maximum injection time of 150 ms. The data was then analyzed using SEQUEST (Thermo Fisher Scientific, San Jose, CA, version v.27, rev. 11.) and Proteome Discoverer (Thermo Scientific, San Jose, CA. version 2.1).

Database Searching

Tandem mass spectra were extracted, and charge states were deconvoluted by Proteome Discoverer version 2.1. Assignment of MS/MS spectra was performed using SequestHT (Thermo Fisher Scientific, San Jose, CA, USA) by

searching the data against a protein database, including all entries from the Uniprot *Drosophila* proteome (UniProt UP00000803, containing 21,041 sequences, download date 10-29-2019) combined with the common contaminants sequences from the Global Proteome Machine. Sequest searches were performed using a parent ion tolerance of 1.25 Da, fragment ion mass tolerance of 1.00005 Da, and requiring each peptides' termini to have trypsin protease specificity while allowing up to two missed cleavages. Carbamidomethylation of cysteine residues (+57.02146 Da) was set as static modification, while TMT tags on peptide N termini/lysine residues (+229.162932 Da), acetylation of the protein Nterminus, and methionine oxidation (+15.99492 Da) was set as variable modification. Reporter Ions Quantifier settings were set to include unique and razor peptides, Quan value correction factors from manufacturer applied, co-isolation threshold 50%, average reporter S/N 10, and no normalization or scaling of the channels.

Proteomic Data Analysis

The unscaled, non-normalized protein-level total reporter ion intensities derived from unique peptides were exported from Proteome Discoverer. Data quality assessment and control, normalization and analyses were performed using R v 4.0.1. Proteins underwent three filtering steps: 1) proteins containing missing values in any condition, 2) proteins with fewer than two unique peptide matches, and 3) proteins identified in only one or two out of the three runs were excluded from the quantitative analysis. Each TMT run was internally scaled, then transformed and analyzed together. Merged data were greatly affected by commonly seen batch effects associated to individual runs. Bioconductor package Limma v 3.44.3 was used to identify sexspecific abundance differences per protein in response to changing gravity conditions relative to ground/earth control by performing an empirical Bayes moderated *t*-test accounting for the seen batch effect caused by each individual TMT run (Ritchie et al., 2015). Calculated p-values were corrected by Benjamini–Hochberg False Discovery Rate (FDR). Statistically significant difference was defined by an FDR cutoff of 0.05.

F. Gene ontology and KEGG analysis

The differentially expressed genes and proteins with FDR adjusted p-values less than 0.05 were used for further analysis. Gene ontology (GO) and KEGG enrichment analyses were performed using Bioconductor package ClusterProfiler v 3.18.0 (Yu et al., 2012) and *Drosophila* database (org.Dm.eg.db version 3.13). Specifically, we used enrichGO and enrichKEGG functions to determine functionally enriched GO categories for are three annotations: biological process (BP), cellular component (CC), and molecular function (MF) and KEGG pathways (Carbon et al., 2021) for all contrasts across both transcriptomics and proteomics datasets. Results were visualized by R packages ggplot2 (Wickham, 2016) and pheatmap (Kolde, 2015). The intersecting genes and proteins within and across the multi-omics platform were plotted using the Upset plot (Khan and Mathelier, 2017). Pathway visualization was performed using the KEGG mapper function provided by Kanehisa Laboratories (https://www.kegg.jp/). Venn diagrams were generated using Venny 2.1 (Oliveros, 2015).

QUANTIFICATION AND STATISTICAL ANALYSIS

Quantification methods for the various assays and parameters are described in the relevant Methods section. Statistical analyses and plot generation were performed using GraphPad Prism software (v. 9.1.0). For Figure 1E, two-tailed Student's t-test was performed to determine statistical significance. Grubbs test was performed on all climbing and immunohistochemistry datasets to remove outliers. In Figures 2, 6 (A–C, F), S3A, and S7, Grubbs test was followed by testing for normal Gaussian distribution *via* the D'AgostinoPearson test except in data with a low sample size (TH and Repo), where the Shapiro-Wilk test for normality was performed. If data were normally distributed, a two-way ANOVA, followed by Tukey's multiple comparison test, was performed to determine statistical significance. *$p < 0.05$, **$p < 0.01$, ***$p < 0.001$.

For Figure 6D, a non-parametric t-test (Mann-Whitney test) was performed to compare all conditions (Earth, SF1g, and SFμg) within their respective time points (R+0, R+25). A value of $p<0.05$ was considered statistically significant. The error bars in the figures represent SEM (Standard Error Mean). All data are means ± SEM ($p < 0.05$, n = 5-12 per group). The number of flies used per experiment is indicated in the figure legend. Inflight behavior analysis was conducted by composing Matlab code using Matlab 2018 (MathWorks, Inc., Natick, MA) and DIPimage (Hendriks et al. 1999).

Supplementary Material

Figure S1

Figure S1 (related to Figure 1A, B): MVP-FLY-01 hardware and mission timeline. (A) Representative image of the MVP *Drosophila* hardware. (B) MVP *Drosophila* unit -12 total units were installed in the MVP, six on each carousel. Each food cylinder was labeled in accordance with the actions detailed in Figure 2. The experiment was launched with flies in chamber 2/cylinder 3 and food in cylinder 3. Food cylinders 2 and 1 were not included in launch orientation. Each food cylinder had two openings, and the outer plastic vessel that contains the aluminum food cylinder had a single opening that rotated back and forth to give flies access to one side of the cylinder at a time. This allowed us to control entry of flies into the food cylinder from only a single adult fly chamber at a time, therefore controlling access to egg laying and allowed for separation of generations. Green arrows indicate the progression of the experiment throughout the mission. (C) Schematic of operations timeline onboard ISS during the experiment. The first yellow section represents the time between the packing of the hardware with flies and the time that the experiment began operation on ISS. The following red sections represent times that the modules were packed in cargo transfer bags, and the experiment was inactive. Colored blocks represent different phases of the experiment, which were separated by cylinder rotations and experiment operations. (Day 5) The MVP unit was powered on, and fruit fly food cylinder 2 was retrieved from 4°C storage and inserted into the module. The launch configuration allowed each module to have a food cylinder in the “food cylinder 3” slot, to support the first generation of flies during launch. After this time (the beige section), the initial generation of flies laid eggs in food cylinder 2. Food cylinder 3 was also temporarily closed, to encourage flies to lay eggs on the new food. (Day 10) Food cylinder 2 was rotated so that it faced chamber 1 (the blue section), and the new generation of eggs that were laid entirely in space would emerge into adults in fly chamber 1. This separates the initial adults from the food that contains the eggs for the next generation. Food cylinder 3 was also reopened to fly chamber 2. This allowed for the emergence of new flies, which were laid starting from Launch 1 day into Fly Chamber 2. (Day 21) Food cylinder 1 was retrieved from 4°C and installed. This allowed the flies emerging from cylinder 2 into fly chamber 1 to have fresh food and start laying the eggs that were ultimately fixed in RNAlater for other experiments on day 29. (Day 29) Cylinder 2 was closed off and rotated back to chamber 2, further preventing flies from emerging into chamber 1. A new food cylinder 1 was replaced to provide flies in chamber 1 with fresh food for the return journey. Chamber 1, at this point, only contained the complete generation of live flies bred entirely in space and returned for ground experiments. These flies were 11-17 days of age upon return. Videos from mission days 13-28 were analyzed for inflight behavioral assessments. (Day 31) A weather delay caused undocking to be pushed by at least 48 hrs. At this time, the flies were re-inserted into the MVP unit (yellow section) to avoid exposure of space 1g on-orbit control to the ISS micro-g for too long before sample return. (Day 33) MVP power was finally shut off for the journey back to Earth.

NIHMS1881633-supplement-Figure_S1.png (957.7KB, png)

Figure S2

Figure S2 (related to Figures 1C–E**): Fly population in adult fly chamber 1.** Red represents the number of flies in a SFμg chamber, and blue represents the number of flies in a SF1g chamber, determined by manual counting. Mission day 13 represents the first day where flies are present in the chamber.

NIHMS1881633-supplement-Figure_S2.png (155.7KB, png)

Figure S3

Figure S3 (related to Figures 2, and 6**)**: **Brain morphological deficits in spaceflight**. (A) Quantification of a total brain area showed a significant decrease in the brain area of SFμg female flies (n=13-16). Two-way ANOVA results are displayed above the histogram. (B) Representative confocal images of fly brain stained with neuronal marker anti-ELAV and marked for neuronal cortex (dashed outer white line) and neuropil area (dashed inner yellow line). (C) Representative images of fly brain stained with anti-ELAV (C.i), anti-8-oxo-dG (C.ii), and anti-CC3 (C.iii), are shown. The representative merged images of anti-ELAV and anti-8-oxo-dG, with the green arrowheads and the inset displaying co-localization (C.iv); and co-staining of anti-ELAV and anti-CC3 (C.v) are shown. Significance calculated by post-hoc test is represented as *$p<0.05$; **** $p<0.0001$. The error bars represent SEM.

NIHMS1881633-supplement-Figure_S3.png (17.4MB, png)

Figure S4

Figure S4 (related to Figures 3, 4, and 5): Overlap of DEG and DEP across conditions and intersection of DEG and DEP. Venn diagram showing the overlap of differentially expressed genes (A) and proteins (B) of SF1g and SFμg males and females compared to the Earth males and females respectively. (C) Venn diagram showing the intersection of DEGs and DEPs in SFμg females. (D) Bar plot of GO analysis of the overlapping genes/proteins showing the distribution of GO terms (adj.p-value<0.05). Different colors represent different GO categories (biological processes (BP), cellular components (CC), and molecular functions (MF)).

NIHMS1881633-supplement-Figure_S4.png (719.3KB, png)

Figure S5

Figure S5 (related to Figures 3, 4, and 5): Principal component analysis (PCA) plot and GO enrichment analysis. (A) Transcriptomics PCA plot of variance stabilized transformed (vst) RNAseq data and (B) Proteomics PCA plot of log2-quantile normalized TMT data. Color represents different experimental conditions and symbols represent male and female flies. The first PC is explained by variance explained by sex differences and the second PC demonstrates the differences across gravity conditions. We see clear separation by sex and experimental condition. Dot plot showing GO terms (adj. p-value<0.05) associated with muscles (C) and cytoskeleton (D) in biological processes, molecular function, and cellular components for SF1g and SFμg conditions (DEPs) compared to Earth control. The color of the dot represents adj. pvalue, and the size represents gene ratio.

NIHMS1881633-supplement-Figure_S5.png (770.1KB, png)

Figure S6

Figure S6 (related to Figures 3, 4, and 5): Aging-related proteins in spaceflight. (A) The enriched GO terms (biological processes) related to aging and behavior are plotted, where the size of the dots represents gene ratio, and the color represents adj.p-value<0.05. (B) Heatmap representation of differential expression (log2[fold-change]) of significantly altered (adj. pvalue<0.05) aging-related proteins in SF1g and SFμg conditions compared to Earth control. The colors in the heatmap represent red being upregulated and blue being downregulated.

NIHMS1881633-supplement-Figure_S6.png (618.8KB, png)

Figure S7

Figure S7 (related to Figure 6): Brain morphological assessment at the R+25 timepoint. A histogram displaying quantification of total brain area (A) showed no difference across conditions (n=12-15), while significant depletion of neuronal cortex area (B) is noted in SFμg compared to both Earth and SF1g controls (n=10-13), specifically in female flies. Quantification of DA neurons (C) showed no change across conditions (n=6-10) at the R+25 timepoint. A dosedependent increase in CC3 labeled apoptotic cells (D) was observed (n=4-6). Repo positive glial cells showed decrease in glial cell numbers in both SF1g and SFug compared to Earth condition (n=6-9), with an increase in number of rosettes (F) in SF1g and SFug compared to Earth conditions (n=6-9). Two-way ANOVA results are displayed above the histogram. Significance calculated by post-hoc test is represented as *p<0.05; **p<0.01; *** p<0.001. The error bars represent SEM.

NIHMS1881633-supplement-Figure_S7.png (346.4KB, png)

Supplementary Table 1

Supplementary.xls 1 (related to Figures 3, 4, and 5): Differentially expressed genes (DEGs) and GO enrichment.

Tab1 (SF1gvsEarth_F): DEGs of SF1g females vs Earth females. **Tab 2** (SF1gvsEarth_F_Enrichment): GO enrichment terms (BP, CC, MF) for SF1g females vs Earth females. **Tab 3** (SF1gvsEarth_M): DEGs of SF1g males vs Earth males. **Tab 4** (SF1gvsEarth_F_Enrichment): GO enrichment terms (BP, CC, MF) for SF1g males vs Earth males. **Tab 5** (SFμgvsEarth_F): DEGs of SFμg females vs Earth females. **Tab 6** (SFμgvsEarth_F_Enrichment): GO enrichment terms (BP, CC, MF) for SFμg females vs Earth females. **Tab 7** (SFμgvsEarth_M): DEGs of SFμg males vs Earth males. **Tab 8** (SFμgvsEarth_F_Enrichment): GO enrichment terms (BP, CC, MF) for SFμg males vs Earth males.

NIHMS1881633-supplement-Supplementary_Table_1.xlsx (189.4KB, xlsx)

Supplementary Table 2

Supplementary.xls 2 (related to Figures 3, 4, and 5): Differentially expressed proteins (DEPs) and GO enrichment.

Tab1 (SF1gvsEarth_F): DEPs of SF1g females vs Earth females. **Tab 2** (SF1gvsEarth_F_Enrichment): GO enrichment terms (BP, CC, MF) for SF1g females vs Earth females. **Tab 3** (SF1gvsEarth_M): DEPs of SF1g males vs Earth males. **Tab 4** (SF1gvsEarth_F_Enrichment): GO enrichment terms (BP, CC, MF) for SF1g males vs Earth males. **Tab 5** (SFμgvsEarth_F): DEPs of SFμg females vs Earth females. **Tab 6** (SFμgvsEarth_F_Enrichment): GO enrichment terms (BP, CC, MF) for SFμg females vs Earth females. **Tab 7** (SFμgvsEarth_M): DEPs of SFμg males vs Earth males. **Tab 8** (SFμgvsEarth_F_Enrichment): GO enrichment terms (BP, CC, MF) for SFμg males vs Earth males.

NIHMS1881633-supplement-Supplementary_Table_2.xlsx (314.5KB, xlsx)

Supplementary Table 3

Supplementary.xls 3 (related to Figure 1 C–E): Inflight behavioral data. Tab1: Raw data. **Tab2:** Normalized to background.

NIHMS1881633-supplement-Supplementary_Table_3.xlsx (62.7KB, xlsx)

Video 1

Supplementary Video 1 (related to Figure 1 C–E): Spaceflight 1g.

Representative videos of fly activity in SF1g adult fly chamber of MVP hardware.

Download video file (14MB, mp4)

Video 2

Supplementary Video 2 (related to Figure 1 C–E): Spaceflight μg.

Representative videos of fly activity in SFμg adult fly chamber of MVP hardware.

Download video file (15.7MB, mp4)

Key resources table

REAGENT or RESOURCE	SOURCE	IDENTIFIER
Antibodies		
Anti-Elav	Developmental Studies Hybridoma Bank	Catalog # 7E8A10
Anti-Cc3	Cell signaling Technology	Catalog # 9661
Anti-8-oxo-dG	R&D systems	Catalog # 4354-MC050
Anti-Repo	Developmental Studies Hybridoma Bank	Catalog # 8D12
Anti-TH	EMD Millipore	Catalog # AB152
Alexa fluor 568 goat anti-mouse	Invitrogen	Catalog # A-11031
Alexa fluor 488 goat anti-rabbit	Invitrogen	Catalog # A-11034
Alexa fluor 633 goat anti-rat	Invitrogen	Catalog # A21094
Experimental models: Organisms/strains		
w1118	Bloomington Stock Center	Stock # 3605
Chemicals, peptides, and recombinant proteins		
Phosphate Buffer Saline	Fisher Scientific	Catalog # BP243820
Triton X-100	Thermo-Fisher Scientific	Catalog # A160460F
Normal Goat Serum	Sigma	Catalog # 566380
Vector Shield	Vector Labs	Catalog # H-1000-10
Endoproteinase Lys-C	Wako	Catalog # 125-05061
Trypsin	Promega	Catalog # V5111
C_{18} Sep-Pak cartridges	Waters	Catalog # WAT020515

REAGENT or RESOURCE	SOURCE	IDENTIFIER
Zorbax 300Extend-C18 column	Agilent	Catalog # 763750902
Acetonitrile	Fisher	Catalog # A9555
Formic Acid	EMD	Catalog # 1.00264
10mM ammonium bicarbonate	Sigma	Catalog # A6141
Critical commercial assays		
Total RNA was extracted using RNA/Protein Purification plus	Norgen	Catalog# 48200
Bicinchoninic acid assay	Thermo-Fisher Scientific	Catalog # 23275
Thermo-Fisher's TMT 10-plex isobaric label kit	Thermo-Fisher Scientific	Catalog # 90061
Deposited data		
Transcriptomics and Proteomics	NASA/GeneLab	GLDS-514 https://genelabdata.ndc.nasa.gov/genelab/accession/GLDS-514/
Inflight behavior analysis	Zenodo	DOI:10.5281/zenodo.6686815
Software and algorithms		
Matlab	Matlab 2018 (MathWorks, Inc., Natick, MA)	MATLAB; RRID:SCR_001622
Image J v1.52g	U. S. National Institutes of Health, Bethesda, Maryland, USA	ImageJ; RRID:SCR_003070
ggplot2 v3.3.1	(Wickham, 2016)	https://ggplot2.tidyverse.org ; RRID:SCR_014601
Trim Galore! v0.6.2	N/A	https://www.bioinformatics.babraham.ac.uk/projects/trim_galore/ , RRID:SCR_011847
STAR v2.7.1a	Dobin et al., 2013	https://github.com/alexdobin/STAR , RRID: SCR_015899

REAGENT or RESOURCE	SOURCE	IDENTIFIER
RSEM v1.3.1	Dobin et al., 2013	https://deweylab.github.io/RSEM/ , RRID: SCR_013027
DESeq2 v1.22.2	Love et al., 2014	https://github.com/mikelove/DESeq2 , RRID: SCR_01568
pheatmap v1.0.12	Kolde; 2015	https://github.com/raivokolde/pheatmap ; RRID:SCR_016418
R package v3.6.1 and v4.0.1	R Core Team (2020)	https://www.rproject.org/ RRID:SCR_001905
Proteome Discoverer v2.1	Thermo Fisher Scientific	Proteome Discoverer; RRID:SCR_014477
Limma v3.44.3	Ritchie et al., 2015	https://www.bioconductor.org/packages/release/bioc/html/limma.html , RRID: SCR_010943
ClusterProfiler v 3.18.0	Yu et al., 2012	clusterProfiler; RRID:SCR_016884
Venny 2.1	N/A	http://bioinfogp.cnb.csic.es/tools/venny/ ; RRID:SCR_016561
Other		
Illumina Novaseq 6000	Illumina, San Diego, CA	https://www.illumina.com
Ultimate 3000 HPLC	Thermo Scientific	https://www.thermofisher.com
Dionex Ultimate 3000	Thermo Scientific	https://www.thermofisher.com
UltiMate 3000 RSLCnano system	Thermo Scientific	https://www.thermofisher.com
Orbitrap Fusion mass spectrometer	Thermo Scientific	https://www.thermofisher.com

Open in a new tab

Acknowledgements

We would like to thank the ISS Research Integration Office at NASA JSC for funding to SB for the validation of the MVP platform (NASA-OZ (2017-2018)). We would like to thank Redwire (previously Techshot, Inc.), for supporting

the mission and developing the hardware used. We gratefully acknowledge assistance from C. Cheung, P. Bhavsar, E. Pane, C. Angadi, E. Cekanaviciute, I. Fernandes, M. Torres. We thank Dr. Alwood and Dr. Govind for careful reading of the manuscript. We would like to thank the flight crew for technical assistance aboard the ISS.

Inclusion and Diversity

We worked to ensure sex balance in the selection of non-human subjects. One or more of the authors of this paper self-identifies as an underrepresented ethnic minority in science.

Footnotes

Declaration of Interests

The authors declare no competing interests.

References

1. Afshinnekoo E, Scott RT, MacKay MJ, Pariset E, Cekanaviciute E, Barker R, Gilroy S, Hassane D, Smith SM, Zwart SR, et al. (2020). Fundamental Biological Features of Spaceflight: Advancing the Field to Enable Deep-Space Exploration. Cell 183, 1162–1184. [DOI] [PMC free article] [PubMed] [Google Scholar]

2. Beheshti A, Miller J, Kidane Y, Berrios D, Gebre SG, and Costes SV (2018). NASA GeneLab Project: Bridging Space Radiation Omics with Ground Studies. Radiat. Res 189, 553–559. [DOI] [PubMed] [Google Scholar]

3. Beheshti A, Shirazi-Fard Y, Choi S, Berrios D, Gebre SG, Galazka JM, and Costes SV (2019). Exploring the Effects of Spaceflight on Mouse Physiology using the Open Access NASA GeneLab Platform. J. Vis. Exp 2019. [DOI] [PubMed] [Google Scholar]

4. Benguría A, Grande E, De Juan E, Ugalde C, Miquel J, Garesse R, and Marco R (1996). Microgravity effects on Drosophila melanogaster behavior and aging. Implications of the IML-2 experiment. J. Biotechnol 47, 191–201. [DOI] [PubMed] [Google Scholar]

5. Bhatti JS, Bhatti GK, and Reddy PH (2017). Mitochondrial dysfunction and oxidative stress in metabolic disorders — A step towards mitochondria based therapeutic strategies. Biochim. Biophys. Acta - Mol. Basis Dis 1863, 1066–1077. [DOI] [PMC free article] [PubMed] [Google Scholar]

6. Bilimoria PM, and Stevens B (2015). Microglia function during brain development: New insights from

animal models. Brain Res. 1617, 7–17. [DOI] [PubMed] [Google Scholar]

7. Block ML, Zecca L, and Hong JS (2007). Microglia-mediated neurotoxicity: Uncovering the molecular mechanisms. Nat. Rev. Neurosci 8, 57–69. [DOI] [PubMed] [Google Scholar]

8. Bondar RL (2005). The Neurolab Spacelab Mission: Neuroscience Research in Space: Results From the STS-90, Neurolab Spacelab Mission. [Google Scholar]

9. Brooks Robey R, Weisz J, Kuemmerle N, Salzberg AC, Berg A, Brown DG, Kubik L, Palorini R, Al-Mulla F, Al-Temaimi R, et al. (2015). Metabolic reprogramming and dysregulated metabolism: Cause, consequence and/or enabler of environmental carcinogenesis? Carcinogenesis 36, S203–S231. [DOI] [PMC free article] [PubMed] [Google Scholar]

10. Bukau B, Weissman J, and Horwich A (2006). Molecular Chaperones and Protein Quality Control. Cell 125, 443–451. [DOI] [PubMed] [Google Scholar]

11. Carbon S, Douglass E, Good BM, Unni DR, Harris NL, Mungall CJ, Basu S, Chisholm RL, Dodson RJ, Hartline E, et al. (2021). The Gene Ontology resource: Enriching a GOld mine. Nucleic Acids Res. 49, D325–D334. [DOI] [PMC free article] [PubMed] [Google Scholar]

12. Casano AM, and Peri F (2015). Microglia: Multitasking specialists of the brain. Dev. Cell 32, 469–477. [DOI] [PubMed] [Google Scholar]

13. Casas-Vila N, Bluhm A, Sayols S, Dinges N, Dejung M, Altenhein T, Kappei D, Altenhein B, Roignant JY, and Butter F (2017). The developmental proteome of Drosophila melanogaster. Genome Res. 27, 1273–1285. [DOI] [PMC free article] [PubMed] [Google Scholar]

14. Cekanaviciute E, Rosi S, and Costes SV (2018). Central nervous system responses to simulated galactic cosmic rays. Int. J. Mol. Sci 19, 1–14. [DOI] [PMC free article] [PubMed] [Google Scholar]

15. Chakraborty R, Vepuri V, Mhatre SD, Paddock BE, Miller S, Michelson SJ, Delvadia R, Desai A, Vinokur M, Melicharek DJ, et al. (2011). Characterization of a drosophila Alzheimer's disease model: Pharmacological rescue of cognitive defects. PLoS One 6, e20799. [DOI] [PMC free article] [PubMed] [Google Scholar]

16. Chan KL, Inan O, Bhattacharya S, and Marcu O (2012). Estimating the speed of Drosophila locomotion using an automated behavior detection and analysis system. Fly (Austin). 6, 205–210. [DOI] [PubMed] [Google Scholar]

17. Clément GR (2017). International roadmap for artificial gravity research. Npj Microgravity 3. [DOI] [PMC free article] [PubMed] [Google Scholar]

18. Clément G, and Traon A.P. Le (2004). Centrifugation as a countermeasure during actual and simulated microgravity: A review. Eur. J. Appl. Physiol 92, 235–248. [DOI] [PubMed] [Google Scholar]

19. Clément GR, Boyle RD, George KA, Nelson GA, Reschke MF, Williams TJ, and Paloski WH (2020). Challenges to the central nervous system during human spaceflight missions to Mars. J. Neurophysiol 123, 2037–2063. [DOI] [PubMed] [Google Scholar]

20. Cronk JC, and Kipnis J (2013). Microglia - The brain's busy bees. F1000Prime Rep. 5, 53. [DOI] [PMC free article] [PubMed] [Google Scholar]

21. Crucian B, Stowe RP, Mehta S, Quiriarte H, Pierson D, and Sams C (2015). Alterations in adaptive immunity persist during long-duration spaceflight. Npj Microgravity 1. [DOI] [PMC free article] [PubMed] [Google Scholar]

22. Cunningham C (2013). Microglia and neurodegeneration: The role of systemic inflammation. Glia 61, 71–90. [DOI] [PubMed] [Google Scholar]

23. Davis CM, DeCicco-Skinner KL, and Hienz RD (2015). Deficits in sustained attention and changes in dopaminergic protein levels following exposure to proton radiation are related to basal dopaminergic function. PLoS One 10. [DOI] [PMC free article] [PubMed] [Google Scholar]

24. DeFelipe J, Arellano JI, Merchán-Pérez A, González-Albo MC, Walton K, and Llinás R (2002). Spaceflight induces changes in the synaptic circuitry of the postnatal developing neocortex. Cereb. Cortex 12, 883–891. [DOI] [PubMed] [Google Scholar]

25. Dobin A, Davis CA, Schlesinger F, Drenkow J, Zaleski C, Jha S, Batut P, Chaisson M, and Gingeras TR (2013). STAR: Ultrafast universal RNA-seq aligner. Bioinformatics 29, 15–21. [DOI] [PMC free article] [PubMed] [Google Scholar]

26. Dutta SM, Hadley MM, Peterman S, Jewell JS, Duncan VD, and Britten RA (2018). Quantitative Proteomic Analysis of the Hippocampus of Rats with GCR-Induced Spatial Memory Impairment. Radiat. Res 189, 136–145. [DOI] [PubMed] [Google Scholar]

27. Euston DR, Gruber AJ, and McNaughton BL (2012). The role of medial prefrontal cortex in memory and decision making. Neuron 76, 1057–1070. [DOI] [PMC free article] [PubMed] [Google Scholar]

28. Feany MB, and Bender WW (2000). A Drosophila model of Parkinson's disease. Nature 404, 394–398. [DOI] [PubMed] [Google Scholar]

29. Fernández-Moreno MA, Farr CL, Kaguni LS, and Garesse R (2007). Drosophila melanogaster as a model system to study mitochondrial biology. Methods Mol. Biol 372, 33–49. [DOI] [PMC free article] [PubMed]

[Google Scholar]

30. Freeman MR (2006). Sculpting the nervous system: Glial control of neuronal development. Curr. Opin. Neurobiol 16, 119–125. [DOI] [PubMed] [Google Scholar]

31. Friedman J (2011). Why Is the Nervous System Vulnerable to Oxidative Stress? In Oxidative Stress and Free Radical Damage in Neurology, (Totowa, NJ: Humana Press;), pp. 19–27. [Google Scholar]

32. Gaofei H, Ying M, Yun Z, De C, Shengyuan X, and Yulin D (2009). SNAREs-related pathways in rat brains under simulated microgravity environment. 3rd Int. Conf. Bioinforma. Biomed. Eng. ICBBE; 2009 18, 1–4. [Google Scholar]

33. Garrett-Bakelman FE, Darshi M, Green SJ, Gur RC, Lin L, Macias BR, McKenna MJ, Meydan C, Mishra T, Nasrini J, et al. (2019a). The NASA twins study: A multidimensional analysis of a year-long human spaceflight. Science (80-.) 364. [DOI] [PMC free article] [PubMed] [Google Scholar]

34. Gilbert R, Torres M, Clemens R, Hateley S, Hosamani R, Wade W, and Bhattacharya S (2020). Spaceflight and simulated microgravity conditions increase virulence of Serratia marcescens in the Drosophila melanogaster infection model. Npj Microgravity 6, 1–9. [DOI] [PMC free article] [PubMed] [Google Scholar]

35. Grimm D, Grosse J, Wehland M, Mann V, Reseland JE, Sundaresan A, and Corydon TJ (2016). The impact of microgravity on bone in humans. Bone 87, 44–56. [DOI] [PubMed] [Google Scholar]

36. Gu Y (2011). Interaction of free radicals, matrix metalloproteinases and caveolin-1 impacts blood-brain barrier permeability. Front. Biosci S3, 1216. [DOI] [PubMed] [Google Scholar]

37. Hall CN, Klein-Flügge MC, Howarth C, and Attwell D (2012). Oxidative phosphorylation, not glycolysis, powers presynaptic and postsynaptic mechanisms underlying brain information processing. J. Neurosci 32, 8940–8951. [DOI] [PMC free article] [PubMed] [Google Scholar]

38. Hammond TG, Benes E, O'Reilly KC, Wolf DA, Linnehan RM, Taher A, Kaysen JH, Allen PL, and Goodwin TJ (2000). Mechanical culture conditions effect gene expression: gravity-induced changes on the space shuttle. Physiol. Genomics 3, 163–173. [DOI] [PubMed] [Google Scholar]

39. Hanisch UK, and Kettenmann H (2007). Microglia: Active sensor and versatile effector cells in the normal and pathologic brain. Nat. Neurosci 10, 1387–1394. [DOI] [PubMed] [Google Scholar]

40. Harrington M (2014). Fruit flies in space. Lab Anim. (NY) 43, 3. [DOI] [PubMed] [Google Scholar]

41. Hateley S, Hosamani R, Bhardwaj SR, Pachter L, and Bhattacharya S (2016). Transcriptomic response of Drosophila melanogaster pupae developed in hypergravity. Genomics 108, 158–167. [DOI] [PubMed]

[Google Scholar]

42. Horie K, Kato T, Kudo T, Sasanuma H, Miyauchi M, Akiyama N, Miyao T, Seki T, Ishikawa T, Takakura Y, et al. (2019). Impact of spaceflight on the murine thymus and mitigation by exposure to artificial gravity during spaceflight. Sci. Reports 2019 91 9, 1–10. [DOI] [PMC free article] [PubMed] [Google Scholar]

43. Hosamani R, Leib R, Bhardwaj SR, Adams CM, and Bhattacharya S (2016). Elucidating the "gravome": Quantitative Proteomic Profiling of the Response to Chronic Hypergravity in Drosophila. J. Proteome Res 15, 4165–4175. [DOI] [PubMed] [Google Scholar]

44. Howe A, Kiffer F, Alexander TC, Sridharan V, Wang J, Ntagwabira F, Rodriguez A, Boerma M, and Allen AR (2019). Long-Term Changes in Cognition and Physiology after Low-Dose 16O Irradiation. Int. J. Mol. Sci 20. [DOI] [PMC free article] [PubMed] [Google Scholar]

45. Hussin M, Ismail MR, and Ahmad MS (2017). Air-conditioned university laboratories: Comparing CO2 measurement for centralized and split-unit systems. J. King Saud Univ. - Eng. Sci 29, 191–201. [Google Scholar]

46. Iijima K, Liu HP, Chiang AS, Hearn SA, Konsolaki M, and Zhong Y (2004). Dissecting the pathological effects of human Aβ40 and Aβ42 in Drosophila: A potential model for Alzheimer's disease. Proc. Natl. Acad. Sci. U. S. A 101, 6623–6628. [DOI] [PMC free article] [PubMed] [Google Scholar]

47. Ikenaga M, Yoshikawa I, Kojo M, Ayaki T, Ryo H, Ishizaki K, Kato T, Yamamoto H, and Hara R (1997). Mutations induced in Drosophila during space flight. Biol. Sci. Sp. = Uchū Seibutsu Kagaku 11, 346–350. [DOI] [PubMed] [Google Scholar]

48. Ikwegbue PC, Masamba P, Oyinloye BE, and Kappo AP (2018). Roles of heat shock proteins in apoptosis, oxidative stress, human inflammatory diseases, and cancer. Pharmaceuticals 11. [DOI] [PMC free article] [PubMed] [Google Scholar]

49. Impey S, Jopson T, Pelz C, Tafessu A, Fareh F, Zuloaga D, Marzulla T, Riparip LK, Stewart B, Rosi S, et al. (2016). Short- and long-term effects of 56Fe irradiation on cognition and hippocampal DNA methylation and gene expression. BMC Genomics 17. [DOI] [PMC free article] [PubMed] [Google Scholar]

50. Inan OT, Etemadi M, Sanchez ME, Marcu O, Bhattacharya S, and Kovacs GTA (2009). A miniaturized video system for monitoring the locomotor activity of walking Drosophila melanogaster in space and terrestrial settings. IEEE Trans. Biomed. Eng 56, 522–524. [DOI] [PubMed] [Google Scholar]

51. Inan OT, Marcu O, Sanchez ME, Bhattacharya S, and Kovacs GTA (2011). A portable system for monitoring the behavioral activity of Drosophila. J. Neurosci. Methods 202, 45–52. [DOI] [PubMed] [Google Scholar]

52. Indo HP, Majima HJ, Terada M, Suenaga S, Tomita K, Yamada S, Higashibata A, Ishioka N, Kanekura T, Nonaka I, et al. (2016). Changes in mitochondrial homeostasis and redox status in astronauts following long stays in space. Sci. Rep 6, 39015. [DOI] [PMC free article] [PubMed] [Google Scholar]

53. Inokuchi H, Fukui K, Kogure K, Takaoki Muneo, Kinoshita K, Izumi R, and Fujimori Y (2007). Planning Guide for Space Experiment Research (Japan Aerospace Exploration Agency Japan Space Forum;). [Google Scholar]

54. Iyer J, Singh MD, Jensen M, Patel P, Pizzo L, Huber E, Koerselman H, Weiner AT, Lepanto P, Vadodaria K, et al. (2018). Pervasive genetic interactions modulate neurodevelopmental defects of the autism-associated 16p11.2 deletion in Drosophila melanogaster. Nat. Commun 9, 2548. [DOI] [PMC free article] [PubMed] [Google Scholar]

55. Khan A, and Mathelier A (2017). Intervene: A tool for intersection and visualization of multiple gene or genomic region sets. BMC Bioinformatics 18, 1–8. [DOI] [PMC free article] [PubMed] [Google Scholar]

56. Kohlhoff KJ, Jahn TR, Lomas DA, Dobson CM, Crowther DC, and Vendruscolo M (2011). The iFly tracking system for an automated locomotor and behavioural analysis of drosophila melanogaster. Integr. Biol 3, 755–760. [DOI] [PMC free article] [PubMed] [Google Scholar]

57. Kolde R (2015). pheatmap: Pretty heatmaps. https://github.com/raivokolde/pheatmap

58. Kononikhin AS, Starodubtseva NL, Pastushkova LK, Kashirina DN, Fedorchenko KY, Brhozovsky AG, Popov IA, Larina IM, and Nikolaev EN (2017). Spaceflight induced changes in the human proteome. Expert Rev. Proteomics 14, 15–29. [DOI] [PubMed] [Google Scholar]

59. Krukowski K, Feng X, Paladini MS, Chou A, Sacramento K, Grue K, Riparip LK, Jones T, Campbell-Beachler M, Nelson G, et al. (2018). Temporary microglia-depletion after cosmic radiation modifies phagocytic activity and prevents cognitive deficits. Sci. Rep 8. [DOI] [PMC free article] [PubMed] [Google Scholar]

60. Lai Polo SH, Saravia-Butler AM, Boyko V, Dinh MT, Chen YC, Fogle H, Reinsch SS, Ray S, Chakravarty K, Marcu O, et al. (2020). RNAseq Analysis of Rodent Spaceflight Experiments Is Confounded by Sample Collection Techniques. IScience 23. [DOI] [PMC free article] [PubMed] [Google Scholar]

61. Lavara-Culebras E, and Paricio N (2007). Drosophila DJ-1 mutants are sensitive to oxidative stress and show reduced lifespan and motor deficits. Gene 400, 158–165. [DOI] [PubMed] [Google Scholar]

62. Liao PC, Lin HY, Yuh CH, Yu LK, and Wang HD (2008). The effect of neuronal expression of heat shock proteins 26 and 27 on lifespan, neurodegeneration, and apoptosis in Drosophila. Biochem. Biophys. Res. Commun 376, 637–641. [DOI] [PubMed] [Google Scholar]

63. Long DM, Frame AK, Reardon PN, Cumming RC, Hendrix DA, Kretzschmar D, and Giebultowicz JM (2020a). Lactate dehydrogenase expression modulates longevity and neurodegeneration in Drosophila melanogaster. Aging (Albany. NY) 12, 10041–10058. [DOI] [PMC free article] [PubMed] [Google Scholar]

64. Long DM, Frame AK, Reardon PN, Cumming RC, Hendrix DA, Kretzschmar D, and Giebultowicz JM (2020b). Lactate dehydrogenase expression modulates longevity and neurodegeneration in Drosophila melanogaster. Aging (Albany. NY) 12, 10041–10058. [DOI] [PMC free article] [PubMed] [Google Scholar]

65. de Luca C, Deeva I, Mariani S, Maiani G, Stancato A, and Korkina L (2009). Monitoring antioxidant defenses and free radical production in space-flight, aviation and railway engine operators, for the prevention and treatment of oxidative stress, immunological impairment, and pre-mature cell aging. Toxicol. Ind. Health 25, 259–267. [DOI] [PubMed] [Google Scholar]

66. Lundby A, Secher A, Lage K, Nordsborg NB, Dmytriyev A, Lundby C, and Olsen JV (2012). Quantitative maps of protein phosphorylation sites across 14 different rat organs and tissues. Nat. Commun 3. [DOI] [PMC free article] [PubMed] [Google Scholar]

67. Machida M, Lonart G, and Britten RA (2010). Low (60 cGy) doses of (56)Fe HZE-particle radiation lead to a persistent reduction in the glutamatergic readily releasable pool in rat hippocampal synaptosomes. Radiat. Res 174, 618–623. [DOI] [PubMed] [Google Scholar]

68. Magistretti PJ, and Allaman I (2015). A cellular perspective on brain energy metabolism and functional imaging. Neuron 86, 883–901. [DOI] [PubMed] [Google Scholar]

69. Mahadevan AD, Hupfeld KE, Lee JK, De Dios YE, Kofman IS, Beltran NE, Mulder E, Bloomberg JJ, Mulavara AP, and Seidler RD (2021). Head-Down-Tilt Bed Rest With Elevated CO 2: Effects of a Pilot Spaceflight Analog on Neural Function and Performance During a Cognitive-Motor Dual Task. Front. Physiol 12. [DOI] [PMC free article] [PubMed] [Google Scholar]

70. Mao, Byrum S, Nishiyama NC, Pecaut MJ, Sridharan V, Boerma M, Tackett AJ, Shiba D, Shirakawa M, Takahashi S, et al. (2018a). Impact of spaceflight and artificial gravity on the mouse retina: Biochemical and proteomic analysis. Int. J. Mol. Sci 19. [DOI] [PMC free article] [PubMed] [Google Scholar]

71. Mao XW, Nishiyama NC, Pecaut MJ, Campbell-Beachler M, Gifford P, Haynes KE, Becronis C, and Gridley DS (2016). Simulated Microgravity and Low-Dose/Low-Dose-Rate Radiation Induces Oxidative Damage in the Mouse Brain. Radiat. Res 185, 647–657. [DOI] [PubMed] [Google Scholar]

72. Mao XW, Nishiyama NC, Campbell-Beachler M, Gifford P, Haynes KE, Gridley DS, and Pecaut MJ (2017). Role of NADPH Oxidase as a Mediator of Oxidative Damage in LowDose Irradiated and Hindlimb-

Unloaded Mice. Radiat. Res 188, 392–399. [DOI] [PubMed] [Google Scholar]

73. Mao XW, Sandberg LB, Gridley DS, Herrmann EC, Zhang G, Raghavan R, Zubarev RA, Zhang B, Stodieck LS, Ferguson VL, et al. (2018b). Proteomic Analysis of Mouse Brain Subjected to Spaceflight. Int. J. Mol. Sci 20. [DOI] [PMC free article] [PubMed] [Google Scholar]

74. Mao XW, Nishiyama NC, Byrum SD, Stanbouly S, Jones T, Holley J, Sridharan V, Boerma M, Tackett AJ, Willey JS, et al. (2020). Spaceflight induces oxidative damage to blood-brain barrier integrity in a mouse model. FASEB J. 34, 15516–15530. [DOI] [PMC free article] [PubMed] [Google Scholar]

75. Marcu O, Lera MP, Sanchez ME, Levic E, Higgins LA, Shmygelska A, Fahlen TF, Nichol H, and Bhattacharya S (2011). Innate Immune Responses of Drosophila melanogaster Are Altered by Spaceflight. PLoS One 6, e15361. [DOI] [PMC free article] [PubMed] [Google Scholar]

76. Martin JR, Ernst R, and Heisenberg M (1998). Mushroom bodies suppress locomotor activity in Drosophila melanogaster. Learn. Mem 5, 179–191. [PMC free article] [PubMed] [Google Scholar]

77. Mattson MP, and Liu D (2002). Energetics and oxidative stress in synaptic plasticity and neurodegenerative disorders. Neuromolecular Med. 2, 215–231. [DOI] [PubMed] [Google Scholar]

78. McDonald J, Stainforth R, Miller J, Cahill T, da Silveira W, Rathi K, Hardiman G, Taylor D, Costes S, Chauhan V, et al. (2020). NASA GeneLab Platform Utilized for Biological Response to Space Radiation in Animal Models. Cancers (Basel). 12. [DOI] [PMC free article] [PubMed] [Google Scholar]

79. Mhatre SD, Michelson SJ, Gomes J, Tabb LP, Saunders AJ, and Marenda DR (2014). Development and characterization of an aged onset model of Alzheimer's disease in Drosophila melanogaster. Exp. Neurol 261, 772–781. [DOI] [PubMed] [Google Scholar]

80. Miller MS, Fortney MD, and Keller TS (2002). An infrared system for monitoring Drosophila motility during microgravity. J. Gravit. Physiol 9, 83–91. [PubMed] [Google Scholar]

81. Ogneva IV, Belyakin SN, Sarantseva SV, Maximova MV, Larina IM, Vico L, and van Loon JJ (2016). The Development Of Drosophila Melanogaster under Different Duration Space Flight and Subsequent Adaptation to Earth Gravity. PLoS One 11, e0166885. [DOI] [PMC free article] [PubMed] [Google Scholar]

82. Overbey EG, Saravia-Butler AM, Zhang Z, Rathi KS, Fogle H, da Silveira WA, Barker RJ, Bass JJ, Beheshti A, Berrios DC, et al. (2021). NASA GeneLab RNA-seq consensus pipeline: standardized processing of short-read RNA-seq data. IScience 24. [DOI] [PMC free article] [PubMed] [Google Scholar]

83. Parihar VK, Allen BD, Tran KK, Chmielewski NN, Craver BM, Martirosian V, Morganti JM, Rosi S, Vlkolinsky R, Acharya MM, et al. (2015). Targeted overexpression of mitochondrial catalase prevents

radiation-induced cognitive dysfunction. Antioxidants Redox Signal. 22, 78–91. [DOI] [PMC free article] [PubMed] [Google Scholar]

84. Parihar VK, Allen BD, Caressi C, Kwok S, Chu E, Tran KK, Chmielewski NN, Giedzinski E, Acharya MM, Britten RA, et al. (2016). Cosmic radiation exposure and persistent cognitive dysfunction. Sci. Rep 6, 34774. [DOI] [PMC free article] [PubMed] [Google Scholar]

85. Parihar VK, Maroso M, Syage A, Allen BD, Angulo MC, Soltesz I, and Limoli CL (2018). Persistent nature of alterations in cognition and neuronal circuit excitability after exposure to simulated cosmic radiation in mice. Exp. Neurol 305, 44–55. [DOI] [PubMed] [Google Scholar]

86. Raber J, Allen AR, Sharma S, Allen B, Rosi S, Olsen RHJ, Davis MJ, Eiwaz M, Fike JR, and Nelson GA (2016). Effects of Proton and Combined Proton and 56Fe Radiation on the Hippocampus. Radiat. Res 185, 20–30. [DOI] [PubMed] [Google Scholar]

87. Raber J, Torres ERS, Akinyeke T, Lee J, Weber Boutros SJ, Turker MS, and Kronenberg A (2018a). Detrimental effects of helium ion irradiation on cognitive performance and cortical levels of MAP-2 in B6D2F1 mice. Int. J. Mol. Sci 19. [DOI] [PMC free article] [PubMed] [Google Scholar]

88. Raber J, Torres ERS, Akinyeke T, Lee J, Weber Boutros SJ, Turker MS, and Kronenberg A (2018b). Detrimental Effects of Helium Ion Irradiation on Cognitive Performance and Cortical Levels of MAP-2 in B6D2F1 Mice. Int. J. Mol. Sci 19. [DOI] [PMC free article] [PubMed] [Google Scholar]

89. Raber J, Yamazaki J, Torres ERS, Kirchoff N, Stagaman K, Sharpton T, Turker MS, and Kronenberg A (2019). Combined effects of three high-energy charged particle beams important for space flight on brain, behavioral and cognitive endpoints in B6D2F1 female and Male mice. Front. Physiol 10. [DOI] [PMC free article] [PubMed] [Google Scholar]

90. Rabin BM, Shukitt-Hale B, Carrihill-Knoll KL, and Gomes SM (2014). Comparison of the effects of partial-or whole-body exposures to 16O particles on cognitive performance in rats. Radiat. Res 181, 251–257. [DOI] [PubMed] [Google Scholar]

91. Rai B, Kaur J, Catalina M, Anand SC, Jacobs R, and Teughels W (2011). Effect of simulated microgravity on salivary and serum oxidants, antioxidants, and periodontal status. J. Periodontol 82, 1478–1482. [DOI] [PubMed] [Google Scholar]

92. Ranjan A, Behari J, and Mallick BN (2014). Cytomorphometric Changes in Hippocampal CA1 Neurons Exposed to Simulated Microgravity Using Rats as Model. Front. Neurol 5, 77. [DOI] [PMC free article] [PubMed] [Google Scholar]

93. Ray S, Gebre S, Fogle H, Berrios DC, Tran PB, Galazka JM, and Costes SV (2019). GeneLab: Omics

database for spaceflight experiments. Bioinformatics 35, 1753–1759. [DOI] [PubMed] [Google Scholar]

94. Ren X, Zou L, Zhang X, Branco V, Wang J, Carvalho C, Holmgren A, and Lu J (2017). Redox Signaling Mediated by Thioredoxin and Glutathione Systems in the Central Nervous System. Antioxidants Redox Signal. 27, 989–1010. [DOI] [PMC free article] [PubMed] [Google Scholar]

95. Ritchie ME, Phipson B, Wu D, Hu Y, Law CW, Shi W, and Smyth GK (2015). Limma powers differential expression analyses for RNA-sequencing and microarray studies. Nucleic Acids Res. 43, e47. [DOI] [PMC free article] [PubMed] [Google Scholar]

96. Ronca AE, Moyer EL, and Talyansky Y et al. (2019). Behavior of mice aboard the International Space Station. Sci Rep 9. [DOI] [PMC free article] [PubMed] [Google Scholar]

97. Ross MD, and Varelas J (2005). Synaptic ribbon plasticity, ribbon size and potential regulatory mechanisms in utricular and saccular maculae. J. Vestib. Res 15, 17–30. [PubMed] [Google Scholar]

98. Roy CS, and Sherrington CS (1890). On the Regulation of the Blood-supply of the Brain. J. Physiol 11, 85–158.17. [DOI] [PMC free article] [PubMed] [Google Scholar]

99. Rutter L, Barker R, Bezdan D, Cope H, Costes SV, Degoricija L, Fisch KM, Gabitto MI, Gebre S, Giacomello S, et al. (2020). A New Era for Space Life Science: International Standards for Space Omics Processing. Patterns 1, 100148. [DOI] [PMC free article] [PubMed] [Google Scholar]

100. Ryczko D, and Dubuc R (2017). Dopamine and the Brainstem Locomotor Networks: From Lamprey to Human. Front. Neurosci 11, 295. [DOI] [PMC free article] [PubMed] [Google Scholar]

101. Salim S (2017). Oxidative Stress and the Central Nervous System. J. Pharmacol. Exp. Ther 360, 201–205. [DOI] [PMC free article] [PubMed] [Google Scholar]

102. Sato K, Tanaka R, Ishikawa Y, and Yamamoto D (2020). Behavioral evolution of Drosophila: Unraveling the circuit basis. Genes (Basel). 11. [DOI] [PMC free article] [PubMed] [Google Scholar]

103. Shiba D, Mizuno H, Yumoto A, Shimomura M, Kobayashi H, Morita H, Shimbo M, Hamada M, Kudo T, Shinohara M, et al. (2017). Development of new experimental platform 'MARS'-Multiple Artificial-gravity Research System-to elucidate the impacts of micro/partial gravity on mice. Sci. Rep 7, 1–10. [DOI] [PMC free article] [PubMed] [Google Scholar]

104. da Silveira WA, Fazelinia H, Rosenthal SB, Laiakis EC, Kim MS, Meydan C, Kidane Y, Rathi KS, Smith SM, Stear B, et al. (2020). Comprehensive Multi-omics Analysis Reveals Mitochondrial Stress as a Central Biological Hub for Spaceflight Impact. Cell 183, 1185–1201.e20. [DOI] [PMC free article] [PubMed] [Google Scholar]

105. Slawson JB, Kim EZ, and Griffith LC (2009). High-resolution video tracking of locomotion in adult Drosophila melanogaster. J. Vis. Exp [DOI] [PMC free article] [PubMed] [Google Scholar]

106. Sokolova IV, Schneider CJ, Bezaire M, Soltesz I, Vlkolinsky R, and Nelson GA (2015). Proton radiation alters intrinsic and synaptic properties of CA1 pyramidal neurons of the mouse hippocampus. Radiat. Res 183, 208–218. [DOI] [PubMed] [Google Scholar]

107. De Sousa Abreu R, Penalva LO, Marcotte EM, and Vogel C (2009). Global signatures of protein and mRNA expression levels. Mol. Biosyst 5, 1512–1526. [DOI] [PMC free article] [PubMed] [Google Scholar]

108. Stauch KL, Purnell PR, Villeneuve LM, and Fox HS (2015). Proteomic analysis and functional characterization of mouse brain mitochondria during aging reveal alterations in energy metabolism. Proteomics 15, 1574–1586. [DOI] [PMC free article] [PubMed] [Google Scholar]

109. Stein TP (2002). Space flight and oxidative stress. Nutrition 18, 867–871. [DOI] [PubMed] [Google Scholar]

110. Straume T, Slaba T, Bhattacharya S, and Braby L (2017). Cosmic-ray interaction data for designing biological experiments in space. Life Sci. Sp. Res 13, 51–59. [DOI] [PubMed] [Google Scholar]

111. Tanner LB, Goglia AG, Wei MH, Sehgal T, Parsons LR, Park JO, White E, Toettcher JE, and Rabinowitz JD (2018). Four Key Steps Control Glycolytic Flux in Mammalian Cells. Cell Syst. 7, 49–62.e8. [DOI] [PMC free article] [PubMed] [Google Scholar]

112. Wallace DC (2005). A mitochondrial paradigm of metabolic and degenerative diseases, aging, and cancer: A dawn for evolutionary medicine. Annu. Rev. Genet 39, 359–407. [DOI] [PMC free article] [PubMed] [Google Scholar]

113. Walls S, Diop S, Birse R, Elmen L, Gan Z, Kalvakuri S, Pineda S, Reddy C, Taylor E, Trinh B, et al. (2020). Prolonged Exposure to Microgravity Reduces Cardiac Contractility and Initiates Remodeling in Drosophila. Cell Rep. 33, 108445. [DOI] [PMC free article] [PubMed] [Google Scholar]

114. Wang Y, Iqbal J, Liu Y, Su R, Lu S, Peng G, Zhang Y, Qing H, and Deng Y (2015). Effects of simulated microgravity on the expression of presynaptic proteins distorting the GABA/glutamate equilibrium - A proteomics approach. Proteomics 15, 3883–3891. [DOI] [PubMed] [Google Scholar]

115. Watts ME, Pocock R, and Claudianos C (2018). Brain Energy and Oxygen Metabolism: Emerging Role in Normal Function and Disease. Front. Mol. Neurosci 11, 216. [DOI] [PMC free article] [PubMed] [Google Scholar]

116. White KE, Humphrey DM, and Hirth F (2010). The dopaminergic system in the aging brain of Drosophila. Front. Neurosci 4, 205. [DOI] [PMC free article] [PubMed] [Google Scholar]

117. Whoolery CW, Walker AK, Richardson DR, Lucero MJ, Reynolds RP, Beddow DH, Clark KL, Shih H-Y, LeBlanc JA, Cole MG, et al. (2017). Whole-Body Exposure to 28Si-Radiation Dose-Dependently Disrupts Dentate Gyrus Neurogenesis and Proliferation in the Short Term and New Neuron Survival and Contextual Fear Conditioning in the Long Term. Radiat. Res 188, 532–551. [DOI] [PMC free article] [PubMed] [Google Scholar]

118. Wickham H (2016). ggplot2: Elegant Graphics for Data Analysis. (Springer-Verlag; New York:). [Google Scholar]

119. Wilson MH, Hargens AR, and Imray CH (2018). Effects of Spaceflight on Astronaut Brain Structure. N. Engl. J. Med 378, 581. [DOI] [PubMed] [Google Scholar]

120. Yamamoto D, and Ishikawa Y (2013). Genetic and neural bases for species-specific behavior in drosophila species. J. Neurogenet 27, 130–142. [DOI] [PubMed] [Google Scholar]

121. Young LR (1999). Artificial gravity considerations for a Mars exploration mission. In Annals of the New York Academy of Sciences, (New York Academy of Sciences), pp. 367–378. [DOI] [PubMed] [Google Scholar]

122. Yu G, Wang LG, Han Y, and He QY (2012). ClusterProfiler: An R package for comparing biological themes among gene clusters. Omi. A J. Integr. Biol 16, 284–287. [DOI] [PMC free article] [PubMed] [Google Scholar]

Associated Data

This section collects any data citations, data availability statements, or supplementary materials included in this article.

Supplementary Materials

Figure S1

Figure S1 (related to Figure 1A, B): MVP-FLY-01 hardware and mission timeline. (A) Representative image of the MVP *Drosophila* hardware. (B) MVP *Drosophila* unit -12 total units were installed in the MVP, six on each carousel. Each food cylinder was labeled in accordance with the actions detailed in Figure 2. The experiment was launched with flies in chamber 2/cylinder 3 and food in cylinder 3. Food cylinders 2 and 1 were not included in launch orientation. Each food cylinder had two openings, and the outer plastic vessel that contains the aluminum food cylinder had a single opening that rotated back and forth to give flies access to one side of the cylinder at a time. This allowed us to control entry of flies into the food cylinder from only a single adult fly chamber at a time, therefore controlling access to egg laying and allowed for separation of generations. Green arrows indicate the progression of the experiment throughout the mission. (C) Schematic of operations timeline onboard ISS during the experiment. The first yellow section represents the time between the packing of the hardware with flies and the time that the experiment began operation on ISS. The following red sections represent times that the modules were packed in cargo transfer bags, and the experiment was inactive. Colored blocks represent different phases of the experiment, which were separated by cylinder rotations and experiment operations. (Day 5) The MVP unit was powered on, and fruit fly food cylinder 2 was retrieved from 4°C storage and inserted into the module. The launch configuration allowed each module to have a food cylinder in the “food cylinder 3” slot, to support the first generation of flies during launch. After this time (the beige section), the initial generation of flies laid eggs in food cylinder 2. Food cylinder 3 was also temporarily closed, to encourage flies to lay eggs on the new food. (Day 10) Food cylinder 2 was rotated so that it faced chamber 1 (the blue section), and the new generation of eggs that were laid entirely in space would emerge into adults in fly chamber 1. This separates the initial adults from the food that contains the eggs for the next generation. Food cylinder 3 was also reopened to fly chamber 2. This allowed for the emergence of new flies, which were laid starting from Launch 1 day into Fly Chamber 2. (Day 21) Food cylinder 1 was retrieved from 4°C and installed. This allowed the flies emerging from cylinder 2 into fly chamber 1 to have fresh food and start laying the eggs that were ultimately fixed in RNAlater for other experiments on day 29. (Day 29) Cylinder 2 was closed off and rotated back to chamber 2, further preventing flies from emerging into chamber 1. A new food cylinder 1 was replaced to provide flies in chamber 1 with fresh food for the return journey. Chamber 1, at this point, only contained the complete generation of live flies bred entirely in space and returned for ground experiments. These flies were 11-17 days of age upon return. Videos from mission days 13-28 were analyzed for inflight behavioral assessments. (Day 31) A weather delay caused undocking to be pushed by at least 48 hrs. At this time, the flies were re-inserted into the MVP unit (yellow section) to avoid exposure of space 1g on-orbit control to the ISS micro-g for too long before sample return. (Day 33) MVP power was finally shut off for the journey back to Earth.

NIHMS1881633-supplement-Figure_S1.png (957.7KB, png)

Figure S2

Figure S2 (related to Figures 1C–E**): Fly population in adult fly chamber 1.** Red represents the number of flies in a SFμg chamber, and blue represents the number of flies in a SF1g chamber, determined by manual counting. Mission day 13 represents the first day where flies are present in the chamber.

NIHMS1881633-supplement-Figure_S2.png (155.7KB, png)

Figure S3

Figure S3 (related to Figures 2, and 6**)**: **Brain morphological deficits in spaceflight**. (A) Quantification of a total brain area showed a significant decrease in the brain area of SFμg female flies (n=13-16). Two-way ANOVA results are displayed above the histogram. (B) Representative confocal images of fly brain stained with neuronal marker anti-ELAV and marked for neuronal cortex (dashed outer white line) and neuropil area (dashed inner yellow line). (C) Representative images of fly brain stained with anti-ELAV (C.i), anti-8-oxo-dG (C.ii), and anti-CC3 (C.iii), are shown. The representative merged images of anti-ELAV and anti-8-oxo-dG, with the green arrowheads and the inset displaying co-localization (C.iv); and co-staining of anti-ELAV and anti-CC3 (C.v) are shown. Significance calculated by post-hoc test is represented as *$p<0.05$; **** $p<0.0001$. The error bars represent SEM.

NIHMS1881633-supplement-Figure_S3.png (17.4MB, png)

Figure S4

Figure S4 (related to Figures 3, 4, and 5): Overlap of DEG and DEP across conditions and intersection of DEG and DEP. Venn diagram showing the overlap of differentially expressed genes (A) and proteins (B) of SF1g and SFμg males and females compared to the Earth males and females respectively. (C) Venn diagram showing the intersection of DEGs and DEPs in SFμg females. (D) Bar plot of GO analysis of the overlapping genes/proteins showing the distribution of GO terms (adj.p-value<0.05). Different colors represent different GO categories (biological processes (BP), cellular components (CC), and molecular functions (MF)).

NIHMS1881633-supplement-Figure_S4.png (719.3KB, png)

Figure S5

Figure S5 (related to Figures 3, 4, and 5): Principal component analysis (PCA) plot and GO enrichment analysis. (A) Transcriptomics PCA plot of variance stabilized transformed (vst) RNAseq data and (B) Proteomics PCA plot of log2-quantile normalized TMT data. Color represents different experimental conditions and symbols represent male and female flies. The first PC is explained by variance explained by sex differences and the second PC demonstrates the differences across gravity conditions. We see clear separation by sex and experimental condition. Dot plot showing GO terms (adj. p-value<0.05) associated with muscles (C) and cytoskeleton (D) in biological processes, molecular function, and cellular components for SF1g and SFμg conditions (DEPs) compared to Earth control. The color of the dot represents adj. pvalue, and the size represents gene ratio.

NIHMS1881633-supplement-Figure_S5.png (770.1KB, png)

Figure S6

Figure S6 (related to Figures 3, 4, and 5): Aging-related proteins in spaceflight. (A) The enriched GO terms (biological processes) related to aging and behavior are plotted, where the size of the dots represents gene ratio, and the color represents adj.p-value<0.05. (B) Heatmap representation of differential expression (log2[fold-change]) of significantly altered (adj. pvalue<0.05) aging-related proteins in SF1g and SFμg conditions compared to Earth control. The colors in the heatmap represent red being upregulated and blue being downregulated.

NIHMS1881633-supplement-Figure_S6.png (618.8KB, png)

Figure S7

Figure S7 (related to Figure 6): Brain morphological assessment at the R+25 timepoint. A histogram displaying quantification of total brain area (A) showed no difference across conditions (n=12-15), while significant depletion of neuronal cortex area (B) is noted in SFμg compared to both Earth and SF1g controls (n=10-13), specifically in female flies. Quantification of DA neurons (C) showed no change across conditions (n=6-10) at the R+25 timepoint. A dosedependent increase in CC3 labeled apoptotic cells (D) was observed (n=4-6). Repo positive glial cells showed decrease in glial cell numbers in both SF1g and SFug compared to Earth condition (n=6-9), with an increase in number of rosettes (F) in SF1g and SFug compared to Earth conditions (n=6-9). Two-way ANOVA results are displayed above the histogram. Significance calculated by post-hoc test is represented as *p<0.05; **p<0.01; *** p<0.001. The error bars represent SEM.

NIHMS1881633-supplement-Figure_S7.png (346.4KB, png)

Supplementary Table 1

Supplementary.xls 1 (related to Figures 3, 4, and 5): Differentially expressed genes (DEGs) and GO enrichment.

Tab1 (SF1gvsEarth_F): DEGs of SF1g females vs Earth females. **Tab 2** (SF1gvsEarth_F_Enrichment): GO enrichment terms (BP, CC, MF) for SF1g females vs Earth females. **Tab 3** (SF1gvsEarth_M): DEGs of SF1g males vs Earth males. **Tab 4** (SF1gvsEarth_F_Enrichment): GO enrichment terms (BP, CC, MF) for SF1g males vs Earth males. **Tab 5** (SFμgvsEarth_F): DEGs of SFμg females vs Earth females. **Tab 6** (SFμgvsEarth_F_Enrichment): GO enrichment terms (BP, CC, MF) for SFμg females vs Earth females. **Tab 7** (SFμgvsEarth_M): DEGs of SFμg males vs Earth males. **Tab 8** (SFμgvsEarth_F_Enrichment): GO enrichment terms (BP, CC, MF) for SFμg males vs Earth males.

NIHMS1881633-supplement-Supplementary_Table_1.xlsx (189.4KB, xlsx)

Supplementary Table 2

Supplementary.xls 2 (related to Figures 3, 4, and 5): Differentially expressed proteins (DEPs) and GO enrichment.

Tab1 (SF1gvsEarth_F): DEPs of SF1g females vs Earth females. **Tab 2** (SF1gvsEarth_F_Enrichment): GO enrichment terms (BP, CC, MF) for SF1g females vs Earth females. **Tab 3** (SF1gvsEarth_M): DEPs of SF1g males vs Earth males. **Tab 4** (SF1gvsEarth_F_Enrichment): GO enrichment terms (BP, CC, MF) for SF1g males vs Earth males. **Tab 5** (SFμgvsEarth_F): DEPs of SFμg females vs Earth females. **Tab 6** (SFμgvsEarth_F_Enrichment): GO enrichment terms (BP, CC, MF) for SFμg females vs Earth females. **Tab 7** (SFμgvsEarth_M): DEPs of SFμg males vs Earth males. **Tab 8** (SFμgvsEarth_F_Enrichment): GO enrichment terms (BP, CC, MF) for SFμg males vs Earth males.

NIHMS1881633-supplement-Supplementary_Table_2.xlsx (314.5KB, xlsx)

Supplementary Table 3

Supplementary.xls 3 (related to Figure 1 C–E): Inflight behavioral data. Tab1: Raw data. **Tab2:** Normalized to background.

NIHMS1881633-supplement-Supplementary_Table_3.xlsx (62.7KB, xlsx)

Video 1

Supplementary Video 1 (related to Figure 1 C–E): Spaceflight 1g.

Representative videos of fly activity in SF1g adult fly chamber of MVP hardware.

Download video file (14MB, mp4)

Video 2

Supplementary Video 2 (related to Figure 1 C–E): Spaceflight μg.

Representative videos of fly activity in SFμg adult fly chamber of MVP hardware.

Download video file (15.7MB, mp4)

Data Availability Statement

- All data reported in this paper will be shared by the lead contact upon request. Transcriptomic and proteomic data (Raw read counts and FASTQ files) are made available at the community-endorsed public repository at NASA Gene Lab.

The code generated during this study is openly available on GitHub at https://github.com/Siddhitamhatre/MVP-inflight-behavior

- Any additional information required to reanalyze the data reported in this paper is available from the Lead Contact upon request.